学位論文

Finite Temperature Crossover in the Lattice Anderson Model

（格子アンダーソン模型における
有限温度のクロスオーバー）

１９９１年
名古屋大学大学院理学研究科

大野義章

Finite Temperature Crossover in the Lattice Anderson Model

Yoshiaki Ōno

Department of Physics, Nagoya University, Nagoya 464-01

Contents

1. Introduction

The strongly correlated electronic systems have been studied intensively during last several years. Among those are the heavy fermion systems realized in the rare earth and actinite compounds. As a model for studying such systems, the Anderson lattice model has been investigated by various methods[1]. Among those methods, we focus our attention on the expansion from the large limit of the orbital degeneracy N (i.e. 1/N-expansion method[2~8]) in the present study. This method has been used in the various types of theoretical studies[9~11], which give the fairly good descriptions of the infinite-U Anderson impurity model. The advantage to use this method is that we obtain the rigorous results in the limit of $N\to\infty$. In the actual system, N is at most 14 but very likely only 6 or less. Nevertheless the results for the thermal properties obtained only through the lowest and the next order terms in the 1/N-expansion show very good agreement with those obtained by the rigorous Bethe-Ansats methods[5,9~11]. As for the Anderson lattice model, several authors have also made similar studies[12~15] but have not been successful yet to obtain a unified theory valid over the whole temperature range. Recently, Jin and Kuroda[16] have applied the boson technique originally introduced by P. Coleman[2] to study the Anderson models with imposing the local constraint strictly. For the Anderson impurity model they have calculated free energy and life time of the conduction electrons rigorously to the most and next dominant terms in powers of 1/N over the whole temperature range, covering the high temperature Kondo regime at

$T>>T_K$ (T_K is the Kondo temperature) and the low temperature Fermi liquid regime at $T<<T_0 \equiv T_K/\log N$. For the Anderson lattice model, they have calculated imaginary part of the t-matrix to find the life time proportional to T^{-2} and of $O((1/N)^3)$ at $T<<T_0$ while proportional to $\log T$ and of $O((1/N)^1)$ at $T>>T_K$[16]. This result seems to suggest that the system makes transition from the Kondo regime to the coherent state (Fermi liquid state) when temperature is lowered, but the detailed properties of the coherent state has remained to be investigated more extensively. Moreover, recent discovery of the oxide superconductors stimulates urgent demand for a theory which describes the coherent regime realized at low temperature in the strongly correlated systems.

In the present study, we propose a model where we can include the inter-site coherence effect at low temperature within the most dominant terms in the 1/N-expansion. Our basic idea is the following: Traditionally, in the degenerate Anderson impurity model, people assume that both of the localized f-state and the conduction bands have the N-fold orbital degeneracies and at the same time that the mixing energy V_{sf} and the density of states of each conduction band are proportional to $(1/N)^{1/2}$ and $(1/N)^0$, respectively. On the other hand, for the degenerate Anderson lattice model, such assumption leads to serious inconveniences: the intersite coherence effect is only from the higher order corrections of O(1/N) and dissappears in the limit $N\to\infty$, and the chemical potential becomes N-dependent in order to keep the total number of electrons to be a constant, and so on[14,16]. In order to avoid such inconveniences, in the present

study, we apply a modified version of the degenerate Anderson lattice model. We divide the total degrees of freedom for the conduction electrons $\{\sigma,k\}(\sigma=\uparrow$ or $\downarrow)$ to N subspaces with $\{m,k_m\}$ where $m=-J,-J+1,\cdots,J$ $(N=2J+1)$. The conduction electron with $|m,k_m\rangle$ is assumed to mix exclusively with the m-th orbital state at each f-site. Correspondingly, the mixing energy V_{sf} and the density of states of the conduction electron in each subspace are assumed to be proportional to $(1/N)^0$ and $(1/N)^1$, respectively. In the actual calculations we apply the boson technique with imposing the local constraint strictly. Then we obtain a set of self-consistent equations to the most dominant terms in the 1/N-expansion, which describes the low temperature coherent state where the conduction electrons and the localized electrons couple strongly with each other to form the heavy fermion bands as well as the high temperature incoherent state where the conduction electrons are scattered randomly by the independent Kondo impurities. The transition between those two states occurs rather continuously without showing any distinct phase transition around a certain temperature T_0 called as coherence temperature. We perform the numerical calculation to solve the self-consistent equations over the whole temperature range in the realistic model with N=6 and to observe the explicit feature of such transition across the intermediate temperature range at $T \gtrsim T_0$. T_0 is given by $T_0 \simeq 0.16E_0$ in the present model, where E_0 is the binding energy at T=0 which corresponds to the Kondo temperature in the single impurity problem. What we observe are: with increasing temperature, the magnitude of the hybridization gap formed in the

coherent state decreases rapidly and the phase volume in the k-space enclosed by the Fermi surface also decreases rapidly, while the inverse of the life time increases linearly with T. At further higher temperature, the hybridization gap turns into the pseudo gap and then the dense Kondo regime is realized when the Fermi level is located inside the pseudo gap.

Recently, several authors[13~15] have investigated the low temperature properties of the degenerate Anderson lattice model employing the functional integral method originally developed by Read and Newns[5]. In their calculations, the low temperature coherent state is described as a broken symmetry state with non-zero anomalous average of the boson field. Therefore, the system exhibits distinct phase transition when it moves between the low temperature coherent state and the high temperature incoherent state[14]. This feature shows significant contrast to results obtained in the present study and to the experimental observation.

In section 2, we present the model and the formulation, and derive a set of integral equations for obtaining the single particle Green's functions to the most dominant terms in the 1/N-expansion. We then give the solution of the equations at low temperature limit. In section 3, we study the thermal and transport properties at low and high temperature limits. In section 4, we present the numerical results for the single particle Green's functions and the thermal and transport properties calculated by using a realistic model with N=6 over the whole temperature range. Finally, we give the conclusions and discussions in section 5.

2. Model and Formulation

We study the infinite-U Anderson lattice model by using the slave-boson technique originally introduced by P. Coleman[2]. Our model is given by

$$H = H_c + H_f + H_{cf} \ , \tag{2.1}$$

$$H_c = \sum_{m=-J}^{J} \sum_{k_m} \varepsilon_{k_m} C^+_{k_m} C_{k_m} \ , \tag{2.2}$$

$$H_f = \sum_i \sum_{m=-J}^{J} \varepsilon_f f^+_{im} f_{im} \ , \tag{2.3}$$

$$H_{cf} = \frac{1}{\sqrt{N_L}} \sum_i \sum_{m=-J}^{J} \sum_{k_m} (V_{k_m} e^{-ik_m \cdot R_i} C^+_{k_m} f_{im} b^+_i + h.c.) \ , \tag{2.4}$$

where m stands for the degrees of freedom due to the spin-orbit degeneracy $N \equiv \sum_{m=-J}^{J} 1 = 2J+1$, and i stands for the lattice sites $N_L \equiv \sum_i 1$. k_m represents the generalized wave vector which is first introduced in Ref.[17] and specifies wave vector as well as spin-orbital degrees of freedom. $C^+_{k_m}$ is the creation operator for the conduction (c-) electron. b^+_i and f^+_{im} are the creation operators for the slave-boson and the pseudo-fermion representing the empty and the singly occupied states of the ith f-site, respectively. The creation operator for the f-electron is given by $f^+_{im} b_i$. The energies ε_f and ε_{k_m} are measured relative to the chemical potential. This model (2.1) is

equivalent to the original infinite-U Anderson lattice model as long as it is treated under the local constraint as

$$\hat{Q}_i \equiv \sum_{m=-J}^{J} f_{im}^{+} f_{im} + b_i^{+} b_i = 1, \quad \text{for all } i . \tag{2.5}$$

The expectation value of an operator $\hat{O}$ under the local constraint (2.5) is given by [2,16~18]

$$\langle \hat{O} \rangle = \lim_{\{\lambda_i\} \to \infty} \langle \hat{O} \prod_i \hat{Q}_i \rangle_\lambda \; / \; \langle \prod_i \hat{Q}_i \rangle_\lambda , \tag{2.6}$$

where $\langle \hat{A} \rangle_\lambda$ is calculated in the grand canonical ensemble for the Hamiltonian H_λ:

$$\langle \hat{A} \rangle_\lambda \equiv \mathrm{Tr}[e^{-\beta H_\lambda} \hat{A}] \; / \; \mathrm{Tr}[e^{-\beta H_\lambda}] , \tag{2.7}$$

$$H_\lambda \equiv H_\lambda^0 + H_{cf} , \tag{2.8}$$

and

$$H_\lambda^0 \equiv H_c + H_f + \sum_i \lambda_i \hat{Q}_i . \tag{2.9}$$

For calculating $\langle \hat{A} \rangle_\lambda$, the perturbation method using the Feynman diagrams is employed, where H_{cf} is treated as a perturbation to the unperturbed Hamiltonian H_λ^0. Then the unperturbed components

of the single particle Green's functions of the c-electron, the slave-boson and the pseudo-fermion are given by

$$G^0_{k_m}(i\omega_n) = (i\omega_n - \varepsilon_{k_m})^{-1} , \tag{2.10}$$

$$B^0_i(i\nu_n) = B^0(i\nu_n - \lambda_i) = (i\nu_n - \lambda_i)^{-1} , \tag{2.11}$$

$$F^0_{im}(i\omega_n) = F^0_m(i\omega_n - \lambda_i) = (i\omega_n - \varepsilon_f - \lambda_i)^{-1} , \tag{2.12}$$

where $\omega_n=(2n+1)\pi T$ and $\nu_n=2n\pi T$ with an integer n and temperature T.

Following Ref.[17], we assume the large limit of the spin-orbit degeneracy, N>>1, while keeping the total degrees of freedom for the conduction electron to be constant:

$$\sum_{m=-J}^{J} \left(\frac{1}{N_L} \sum_{k_m} 1\right) = 2 , \tag{2.13}$$

and include the most dominant terms in power of 1/N in each step of calculation. Then, to the most dominant terms, the c-electron, the slave-boson and the pseudo fermion Green's functions are given by the Dyson equations illustrated in Fig.1, whose analytic forms are given by

$$G_{k_m}(i\omega_n) \simeq [G^0_{k_m}(i\omega_n)^{-1} - \Sigma_{k_m}(i\omega_n)]^{-1} , \tag{2.14}$$

$$B(i\nu_n - \lambda_i) \simeq [B^0(i\nu_n - \lambda_i)^{-1} - \Pi(i\nu_n - \lambda_i)]^{-1} , \tag{2.15}$$

$$F_m(i\omega_n-\lambda_i) \simeq F_m^0(i\omega_n-\lambda_i) \ , \tag{2.16}$$

where the self-energy parts are given by

$$\Sigma_{k_m}(i\omega_n) \equiv |V_{k_m}|^2 \, P_m(i\omega_n) \ , \tag{2.17}$$

$$\Pi(i\nu_n-\lambda_i) \equiv \frac{1}{N_L} \sum_m \sum_{k_m} |V_{k_m}|^2 \, T \sum_{\omega_n'} F_m^0(i\omega_n',+i\nu_n-\lambda_i) G_{k_m}(i\omega_n') \ , \tag{2.18}$$

with

$$P_m(i\omega_n) \equiv \lim_{\lambda_i \to \infty} [-T \sum_{\nu_n'} F_m^0(i\omega_n+i\nu_n',-\lambda_i) B(i\nu_n',-\lambda_i)/\langle \hat{Q}_i \rangle_\lambda] \ . \tag{2.19}$$

In eq.(2.19) $\langle \hat{Q}_i \rangle_\lambda$ is defined, from eq.(2.5), by

$$\langle \hat{Q}_i \rangle_\lambda \equiv \sum_m \langle \hat{n}_{fim} \rangle_\lambda + \langle \hat{n}_{bi} \rangle_\lambda \ , \tag{2.20}$$

where $\langle \hat{n}_{fim} \rangle_\lambda \equiv \langle f_{im}^+ f_{im} \rangle_\lambda$ and $\langle \hat{n}_{bi} \rangle \equiv \langle b_i^+ b_i \rangle$. Here we note that when we write eq.(2.14) for G_{k_m} we have included some unphysical terms containing more than one closed loops of F_{im}^0 and B_i referred to a site i artificially in order to get a simple expression as (2.14) with (2.17) and (2.19). When the limit $\lambda_i \to \infty$ is taken according to eq.(2.6), such terms vanish automatically. Therefore such unphysical terms should be subtracted in the final result. However, as shown in Ref.[17], they contribute only to higher

order corrections in the 1/N-expansion of the present model. Actually unphysical terms including such (n+1) closed loops are accompanied by n folds k_m summation, as shown in Fig.2, which yields an additional factor of order of $(1/N)^n$ by considering the assumption (2.13).

To the most dominant terms in the 1/N-expansion, the diagrams contributing to $\sum_m \langle \hat{n}_{fim} \rangle_\lambda$ and $\langle \hat{n}_{bi} \rangle_\lambda$ are illustrated in Fig.3 whose explicit forms are given by

$$\langle \hat{n}_{fim} \rangle_\lambda \simeq T \sum_{\omega_n} F_m^0(i\omega_n - \lambda_i)$$

$$- \frac{1}{N_L} \sum_{k_m} |V_{k_m}|^2 T^2 \sum_{\omega_n \nu_n,} [F_m^0(i\omega_n + i\nu_n, -\lambda_i)]^2 G_{k_m}(i\omega_n) B(i\nu_n, -\lambda_i) \ , \tag{2.21}$$

$$\langle \hat{n}_{bi} \rangle_\lambda \simeq - T \sum_{\nu_n} B(i\nu_n - \lambda_i) \ . \tag{2.22}$$

Substituting eqs.(2.21) and (2.22) into eq.(2.20), we obtain $\langle \hat{Q}_i \rangle_\lambda$, to the most dominant terms, as

$$\langle \hat{Q}_i \rangle_\lambda \simeq \sum_m T \sum_{\omega_n} F_m^0(i\omega_n - \lambda_i)$$

$$+ T \sum_{\nu_n} B(i\nu_n - \lambda_i) \frac{d}{d(i\nu_n)} \Pi(i\nu_n - \lambda_i) - T \sum_{\nu_n} B(i\nu_n - \lambda_i)$$

$$= \sum_m T \sum_{\omega_n} F_m^0(i\omega_n - \lambda_i) - T \sum_{\nu_n} \frac{d}{d(i\nu_n)} \log[B(i\nu_n - \lambda_i)^{-1}] \ . \tag{2.23}$$

Now we perform the analytic continuation from the coupled equations (2.14)~(2.19) and (2.23) to the following integral equations:

$$\mathrm{Im}\Sigma_{k_m}(\omega+i0_+) = |V_{k_m}|^2\ \mathrm{Im}B(-\omega+i0_+)(e^{\beta\omega}+1)/\Psi_Q(T)\ , \tag{2.24}$$

$$\mathrm{Im}\Pi(-\omega+i0_+) = \frac{1}{N_L}\sum_{mk_m}|V_{k_m}|^2\mathrm{Im}G_{k_m}(\omega+i0_+)f(\omega)\ , \tag{2.25}$$

$$\mathrm{Im}G_{k_m}(\omega+i0_+) = \frac{\mathrm{Im}\Sigma_{k_m}(\omega+i0_+)}{[\omega-\varepsilon_{k_m}-\mathrm{Re}\Sigma_{k_m}(\omega)]^2+[\mathrm{Im}\Sigma_{k_m}(\omega+i0_+)]^2} \tag{2.26}$$

$$\mathrm{Im}B(-\omega+i0_+) = \frac{\mathrm{Im}\Pi(-\omega+i0_+)}{[\varepsilon_f-\omega-\mathrm{Re}\Pi(-\omega)]^2+[\mathrm{Im}\Pi(-\omega+i0_+)]^2} \tag{2.27}$$

with

$$\mathrm{Re}\Sigma_{k_m}(\omega) = -\frac{1}{\pi}P\int_{-\infty}^{\infty}d\omega'\ \frac{1}{\omega-\omega'}\ \mathrm{Im}\Sigma_{k_m}(\omega'+i0_+)\ , \tag{2.28}$$

$$\mathrm{Re}\Pi(-\omega) = \frac{1}{\pi}P\int_{-\infty}^{\infty}d\omega'\ \frac{1}{\omega-\omega'}\ \mathrm{Im}\Pi(-\omega'+i0_+)\ , \tag{2.29}$$

and

$$\Psi_Q(T) \equiv \lim_{\lambda_i\to\infty}[e^{\beta(\lambda_i+\varepsilon_f)}\langle\hat{Q}_i\rangle_\lambda]$$

$$= N + \frac{\beta}{\pi}\int_{-\infty}^{\infty} d\omega\ [\frac{\pi}{2} - \arctan\ (\frac{\varepsilon_f - \omega - \mathrm{Re}\Pi(-\omega)}{\mathrm{Im}\Pi(-\omega+i0_+)})]e^{\beta\omega}\ , \tag{2.30}$$

where the energy ω in B and Π is measured relative to ε_f; $f(\omega)\equiv(e^{\beta\omega}+1)^{-1}$ is the Fermi distribution function and $\beta\equiv 1/T$.

At the low temperature limit, the solution of the coupled equations (2.14)~(2.19) and (2.23) has been obtained[17], and here we rewrite the results by using the spectral functions of eqs.(2.24)~(2.30). First the spectral function of the slave-boson is assumed to be given by

$$-\frac{1}{\pi}\mathrm{Im}B(-\omega+i0_+) \simeq a(T)\delta(\omega-E_0(T)) + C(\omega) \quad \text{at } T << E_0\ , \tag{2.31}$$

where the binding energy $E_0(T)$ and the residue $a(T)$ are determined by

$$\mathrm{Re}B(-E_0(T))^{-1} = \varepsilon_f - E_0(T) - \mathrm{Re}\Pi(-E_0(T)) = 0\ , \tag{2.32}$$

$$\frac{1}{a(T)} = -\frac{d}{d\omega}\mathrm{Re}B(-\omega)^{-1}\Big|_{\omega=E_0(T)} = 1 + \frac{d}{d\omega}\mathrm{Re}\Pi(-\omega)\Big|_{\omega=E_0(T)}\ , \tag{2.33}$$

and $E_0>0$ is the binding energy at T=0 which corresponds to the Kondo temperature T_K in the single impurity problem. In eq.(2.31) $C(\omega)$ represents the continuous spectrum for $\omega \lesssim T << E_0(T)$; this is easily found by eq.(2.27) and $f(\omega)$ in eq.(2.25). Here we note that, from the sum rule of the spectral function of the

slave-boson, the residue $a(T)<1$, i.e., $\frac{d}{d\omega}\mathrm{Re}\Pi(-\omega)|_{\omega=E_0(T)}>0$, hence $(\varepsilon_f-\omega-\mathrm{Re}\Pi(-\omega))$ changes its sign at $\omega=E_0(T)$. Using this in eq.(2.30) we obtain

$$\Psi_Q(T) = N + \beta \int_T^{E_0(T)} d\omega\, e^{\beta\omega} + O(1)$$

$$\simeq N + e^{\beta E_0(T)} \quad \text{at } T << E_0 \,, \tag{2.34}$$

where the terms of O(1) are neglected in comparison with the term, $N+e^{\beta E_0(T)}>>1$. Substituting eqs.(2.31) and (2.34) into eq.(2.24) and using eq.(2.28) we obtain the c-electron self-energy as

$$\mathrm{Im}\Sigma_{k_m}(\omega+i0_+) \simeq |V_{k_m}|^2[a(T)\delta(\omega-E_0(T))+C(\omega)](e^{\beta\omega}+1)/(N+e^{\beta E_0(T)})$$

$$\simeq |V_{k_m}|^2\, a(T)\varphi(T)\delta(\omega-E_0(T)) \quad \text{at } T << E_0 \,, \tag{2.35a}$$

$$\mathrm{Re}\Sigma_{k_m}(\omega) \simeq |V_{k_m}|^2\, a(T)\varphi(T)/(\omega-E_0(T)) \quad \text{at } T << E_0 \,, \tag{2.35b}$$

with

$$\varphi(T) \equiv \frac{1 + e^{\beta E_0(T)}}{N + e^{\beta E_0(T)}} \simeq (N^{1-T_0/T} + 1)^{-1} \tag{2.36}$$

$$\simeq \begin{cases} O(1) & \text{at } T \lesssim T_0 \ , \qquad (2.37a) \\ O(1/N) & \text{at } T >> T_0 \qquad (2.37b) \end{cases}$$

where

$$T_0 \equiv E_0(T_0) \ / \ \ell og \ N \ . \qquad (2.38)$$

In deriving eq.(2.35) the terms coming from the continuum $C(\omega)$ are neglected, because $C(\omega) \simeq 0$ for $\omega \gtrsim T$ and $C(\omega) \sim O(1)$ for $\omega \lesssim T$ are in higher orders compared with $(N+e^{\beta E_0(T)}) >> 1$. Substituting eq.(2.35) into eq.(2.14) c-electron Green's function is given by

$$G_{k_m}(i\omega_n) \simeq [i\omega_n - \varepsilon_{k_m} - |V_{k_m}|^2 \ a(T)\varphi(T)/(i\omega_n - E_0(T))]^{-1} \quad \text{at } T << E_0 . \qquad (2.39)$$

Next we calculate the physical f-electron Green's function defined by

$$G^f_{ijm}(i\omega_n) \equiv \lim_{\lambda_i, \lambda_j \to \infty} [G^{f,\lambda}_{ijm}(i\omega_n) / \langle \hat{Q}_i \hat{Q}_j \rangle_\lambda] \ , \qquad (2.40)$$

with

$$G^{f,\lambda}_{ijm}(i\omega_n) \equiv - \int_0^\beta e^{i\omega_n \tau} \langle T_\tau [b^+_i(\tau) f_{im}(\tau) f^+_{jm}(0) b_j(0)] \rangle_\lambda \ d\tau \ . \qquad (2.41)$$

The lowest order contribution to $G^{f,\lambda}_{ijm}$ in the 1/N-expansion comes from the diagrams shown in Fig.4, whose Fourier transform is given by

$$G^f_{k_m}(i\omega_n) \simeq P_m(i\omega_n) + \{P_m(i\omega_n)\}^2 |V_{k_m}|^2 G_{k_m}(i\omega_n)$$

$$= [P_m(i\omega_n)^{-1} - |V_{k_m}|^2 G^0_{k_m}(i\omega)]^{-1} \qquad (2.42a)$$

$$\simeq a(T)\varphi(T)/[i\omega_n - E_0(T) - |V_{k_m}|^2 a(T)\varphi(T)/(i\omega_n - \varepsilon_{k_m})]$$

$$\text{at } T \ll E_0 \ , \qquad (2.42b)$$

where P_m is defined by eq.(2.19) and we have used eq.(2.35b) in deriving eq.(2.42b). The above results show that the present model describes the coherent regime with the quasi-particle (renormalized) bands whose energies are given by the poles of eqs.(2.39) or (2.42b) at low temperature $T \lesssim T_0$:

$$E^{\pm}_{k_m}(T) = \frac{1}{2}\left[\varepsilon_{k_m} + E_0(T) \pm \sqrt{(\varepsilon_{k_m} - E_0(T))^2 + 4a(T)\varphi(T)|V_{k_m}|^2}\ \right] , \qquad (2.43)$$

The quasi-particle band energies $E^{\pm}_{k_m}$ as functions of k_m are illustrated in Fig.5. On the other hand, at high temperature $T \gg T_0$, the present model also describes the incoherent regime with the bare c-electron band and the localized f-electrons, where $G_{k_m} \sim G^0_{k_m} + O(1/N)$ and $G^f_{k_m} \sim O(1/N)$ (see Sec.3.3). In this sense T_0 has been called the coherence temperature in Ref.[17]. Here we show that the Luttinger sum rule[21] is held within $O((1/N)^0)$ in the present model[17]. Following the procedure given in eq.(2.6), we calculate the average number of the c- and f-electrons to the lowest order contribution in the 1/N-

expansion. Using eqs.(2.14), (2.21) and (2.6) we obtain

$$n_c \equiv \frac{1}{N_L} \sum_{mk_m} \langle C^+_{k_m} C_{k_m} \rangle = \frac{1}{N_L} \sum_{k_m} [T \sum_{\omega_n} G_{k_m}(i\omega_n) e^{i\omega_n 0_+}] , \qquad (2.44)$$

$$n_f \equiv \lim_{\lambda_i \to \infty} [\Sigma \langle \hat{n}_{fim} \rangle_\lambda / \langle \hat{Q}_i \rangle_\lambda]$$

$$= n_f^0 + \Delta n_f^{(0)} , \qquad (2.45)$$

with

$$n_f^0 \equiv \sum_m \lim_{\lambda_i \to \infty} [T \sum_{\omega_n} F^0_m(i\omega_n - \lambda_i) / \langle \hat{Q}_i \rangle_\lambda] = N/\Psi_Q(T) , \qquad (2.46a)$$

$$\Delta n_f^{(0)} \equiv \frac{1}{N_L} \sum_{mk_m} [-T \sum_{\omega_m} G_{k_m}(i\omega_n) \frac{d}{d(i\omega_n)} \Sigma_{k_m}(i\omega_n)] , \qquad (2.46b)$$

where n_f^0 is the number of the bare f-electron given by the diagram of Fig.3(a) which corresponds to the incoherent part of the f-electron, while $\Delta n_f^{(0)}$ is the zeroth order contribution for the number of the f-electron given by the diagram of Fig.3(b) which corresponds to the coherent part of the f-electron. In deriving eq.(2.45), eq.(2.17) with eq.(2.19) have been used for $\Sigma_{k_m}(i\omega_n)$. Combining eqs.(2.44) and (2.45) yields

$$n_c + n_f = \frac{1}{N_L}\sum_{mk_m}\left[T\sum_{\omega_n}\frac{d}{d(i\omega_n)}\log[G_{k_m}(i\omega_n)^{-1}]\right] + n_f^0 . \quad (2.47)$$

From eqs.(2.34) and (2.35a) we find $n_f^0=0$ and $\mathrm{Im}\Sigma_{k_m}(\omega+i0_+)\big|_{\omega=0}=0$ at T=0. Hence eq.(2.47) is rewritten as

$$n_c + n_f = \frac{1}{N_L}\sum_{mk_m}\theta(-\varepsilon_{k_m}-\Sigma_{k_m}(0)) = \frac{1}{N_L}\sum_{mk_m}\theta(-E^-_{k_m}) , \quad \text{at } T = 0 . \quad (2.48)$$

Eq.(2.48) means that the Fermi surface in the k-space is determined by the total number of c- and f-electrons at T=0; this is nothing but the Luttinger sum rule. In the present model of the large N limit given in eq.(2.13), we obtain the heavy Fermi liquid state with the coherent renormalized bands which obeys the Luttinger sum rule at low temperature $T\ll T_0$ within the approximation to the lowest order of the 1/N-expansion. This shows a quite contrast to the traditional models of the large N limit.

3. Properties at Low and High Temperature Regimes ($T\ll E_0$ and $T\gg E_0$)

Here we study the thermal and transport properties. In this section the chemical potential μ is explicitly written as $\varepsilon_{k_m}=\xi_{k_m}-\mu$ and $\varepsilon_f=\varepsilon_f^0-\mu$. Further we assume a k_m-independent hybridization: $V_{k_m}=V$, and a constant density of states for the c-electron: $\rho_m^0(\xi)\equiv(1/N_L)\Sigma_{D\,k_m}\delta(\xi-\xi_{k_m})=(ND)^{-1}$ for $-D<\xi<D$ (we note that eq.(2.13) reads $N\int_{-D}^{} d\xi\,\rho_m^0(\xi)=2$ under the present assumption).

Then the imaginary part of the self-energy of the slave-boson in eq.(2.25) is given by

$$\mathrm{Im}\Pi(-\omega+i0_+) = -\tilde{\Delta}(\omega)f(\omega) \ , \tag{3.1}$$

with

$$\tilde{\Delta}(\omega) \equiv \pi N\tilde{\rho}_m(\omega)V^2 \ , \tag{3.2}$$

where $\tilde{\rho}_m$ is the renormalized density of states for the c-electron given by

$$\tilde{\rho}_m(\omega) \equiv \frac{1}{N_L}\sum_{k_m}[-\frac{1}{\pi}\,\mathrm{Im}\,G_{k_m}(\omega+i0_+)]$$

$$= \rho_m^0\,\frac{1}{\pi}\,[\arctan\,(\frac{\omega+\mu-\mathrm{Re}\Sigma(\omega)+D}{-\mathrm{Im}\Sigma(\omega+i0_+)+0_+}) - \arctan(\frac{\omega+\mu-\mathrm{Re}\Sigma(\omega)-D}{-\mathrm{Im}\Sigma(\omega+i0_+)+0_+})] \ . \tag{3.3}$$

In deriving the last line in (3.3) use has been made of eq.(2.26). From eq.(2.35) with (2.37), we find the lowest order contribution to $\tilde{\rho}_m$ in the 1/N-expansion:

$$\tilde{\rho}_m(\omega) \simeq \begin{cases} \rho_m^0, \text{ for } E^{+}_{-\,\mathrm{min.}}(T) < \omega < E^{+}_{-\,\mathrm{max.}}(T) \quad (\text{at } T << E_0) \ , & (3.4a) \\ \rho_m^0, \text{ for } -D-\mu(T) < \omega < D-\mu(T) \quad (\text{at } T >> E_0) \ . & (3.4b) \end{cases}$$

where E_0 is the binding energy of the resonance state defined by eq.(2.32). In eq.(3.4a) $E^{+}_{-\,\mathrm{min.}}$ and $E^{+}_{-\,\mathrm{max.}}$ are the lower and upper

band edges of the renormalized bands shown in eq.(2.43) or Fig.5, and explicitly written as

$$E^{\mp}_{min.}(T) = \frac{1}{2}\left[-D-\mu(T)+E_0(T) \mp \sqrt{(-D-\mu(T)-E_0(T))^2 + 4a(T)\varphi(T)V^2}\right] , \tag{3.5a}$$

$$E^{\mp}_{max.}(T) = \frac{1}{2}\left[D-\mu(T)+E_0(T) \mp \sqrt{(D-\mu(T)-E_0(T))^2 + 4a(T)\varphi(T)V^2}\right] . \tag{3.5b}$$

Substituting eq.(3.1) together with eq.(3.3) or (3.4) into eq.(2.29) we obtain the real part of Π

$$Re\Pi(-\omega) \simeq \frac{\Delta_0}{\pi}\left[\log\left|\frac{2\pi T}{\omega_c(T)+\omega}\right| + Re\Psi\left(\frac{1}{2} + i\frac{\omega}{2\pi T}\right)\right] , \tag{3.6}$$

where

$$\omega_c(T) \simeq \begin{cases} |E^{-}_{min.}(T)| & (\text{at } T << E_0) , \quad (3.7a) \\ |D+\mu(T)| & (\text{at } T >> E_0) , \quad (3.7b) \end{cases}$$

$$\Delta_0 \equiv \pi N \rho^0_m V^2 = \pi \frac{V^2}{D} , \tag{3.8}$$

and Ψ is the di-gamma function. Here we note that $Re\Pi$ has the same form both at $T<<E_0$ and at $T>>E_0$ as shown in eq.(3.6), while, at the intermediate temperature, it has rather complicated form different from eq.(3.6) (see Sec. 4). Substituting eq.(3.6) into eqs.(2.32) and (2.33), we obtain equations to determine the

binding energy and the residue of the resonance state at T=0,

$$\varepsilon_f - E_0 - \frac{\Delta_0}{\pi} \log \left(\frac{E_0}{|E^-_{min.}|+E_0}\right) = 0 \ , \tag{3.9}$$

$$a = \left[1 + \frac{\Delta_0}{\pi} \frac{|E^-_{min.}|}{E_0(|E^-_{min.}|+E_0)}\right]^{-1} \ , \tag{3.10}$$

where $E^-_{min.} \equiv E^-_{min.}(0)$[17]. In Fig.6, the binding energy E_0 and the residue a at T=0 are plotted as functions of the total number of electrons per unit cell n for given values of D, V and ε_f^0. Here $n \equiv n_c + n_f$ with the number of the c-electron n_c and that of the f-electron n_f and will be calculated in Sec. 3.1.

The spectral function of the slave-boson is now evaluated by substituting eqs.(3.1) and (3.6) into eq.(2.27) and is given at low temperature $T \ll E_0$ as

$$\mathrm{Im}B(-\omega+i0_+) \simeq \begin{cases} -\dfrac{a(T)\Gamma(T)}{(\omega-E_0(T))^2+\Gamma(T)^2} & (\text{at } \omega \simeq E_0(T) \gg T) \ , \quad (3.11a) \\ -\dfrac{\tilde{\Delta}(\omega)f(\omega)}{[E_0(T)-\omega-\frac{\Delta_0}{\pi}\log(\frac{2\pi T}{E_0(T)})-\frac{\Delta_0}{\pi}\mathrm{Re}\Psi(\frac{1}{2}+i\frac{\omega}{2\pi T})]^2+[\tilde{\Delta}(\omega)f(\omega)]^2} & (\text{at } \omega \lesssim T) \ , \quad (3.11b) \end{cases}$$

where

$$\Gamma(T) \equiv - a(T)\mathrm{Im}\Pi(-E_0(T)+i0_+)$$

$$\simeq a(T)\tilde{\Delta}(E_0(T))f(E_0(T)) \tag{3.12}$$

is a half width of the resonance level. As shown in eq.(3.5) or Fig.5, the resonance level at $\omega=E_0(T)$ is inside the hybridization gap, hence $\tilde{\Delta}(E_0(T))$ is small at $T<<E_0$, moreover $f(E_0(T))<<1$, at $T<<E_0$. Therefore, $\Gamma(T)$ is extremely small at $T<<E_0$. Thus the assumption, eq.(2.31), is justified. On the other hand, as temperature goes up, the width of the resonance level becomes broader, and finally at $T\gtrsim E_0$ the resonance level and the continuum overlap with each other to form a single broad peak. Finally at high temperature $T>>E_0$ we obtain

$$\mathrm{Im}B(-\omega+i0_+) \simeq -\frac{\Delta_0 f(\omega)}{[E_0(T)-\omega-\frac{\Delta_0}{\pi}\log\left|\frac{2\pi T}{E_0(T)}\right|-\frac{\Delta_0}{\pi}\mathrm{Re}\Psi(\frac{1}{2}+i\frac{\omega}{2\pi T})]^2+[\Delta_0 f(\omega)]^2}\,. \tag{3.13}$$

Substituting eqs.(3.1) and (3.6) into eq.(2.30), $\Psi_Q(T)$ is written as

$$\Psi_Q(T) = N + \Phi(T) \tag{3.14}$$

with

$$\Phi(T) \simeq \begin{cases} e^{\beta E_0(T)} & (\text{at } T << E_0)\,, \end{cases} \tag{3.15a}$$

$$\left\{\frac{\beta}{\pi}\int_{-\infty}^{\infty}d\omega[\frac{\pi}{2}-\arctan(\frac{E_0(T)-\omega-\frac{\Delta_0}{\pi}\log\left|\frac{2\pi T}{E_0(T)}\right|-\frac{\Delta_0}{\pi}\mathrm{Re}\Psi(\frac{1}{2}+i\frac{\omega}{2\pi T})}{-\Delta_0 f(\omega)})]e^{\beta\omega}.\right.$$

$$\left.(\text{at } T >> E_0)\ .\right. \qquad (3.15b)$$

$\Psi_Q(T)$ at $T<<E_0$ has already been obtained in eq.(2.34) in a more general case.

3.1 Number of the f- and the conduction electrons

Following the procedure given in eq.(2.6), we calculate the average number of the slave-boson (empty f-site) n_b and that of the f-electron n_f. By using eqs.(2.21)~(2.23), the lowest order contributions to n_b and n_f in the 1/N-expansion are given by

$$n_b(T) = \lim_{\lambda_i\to\infty}[\langle\hat{n}_{bi}\rangle_\lambda/\langle\hat{Q}_i\rangle_\lambda] = \Psi_b(T)/\Psi_Q(T)\ , \qquad (3.16a)$$

$$n_f(T) = \lim_{\lambda_i\to\infty}[\Sigma_m\langle\hat{n}_{fim}\rangle_\lambda/\langle\hat{Q}_i\rangle_\lambda] = 1 - \Psi_b(T)/\Psi_Q(T)\ , \qquad (3.16b)$$

with

$$\Psi_b(T) \equiv \lim_{\lambda_i\to\infty}[e^{\beta(\lambda_i+\varepsilon_f)}\langle n_{bi}\rangle_\lambda]$$

$$= -\frac{1}{\pi}\int_{-\infty}^{\infty}d\omega\ \mathrm{Im}B(-\omega+i0_+)e^{\beta\omega}\ . \qquad (3.17)$$

Substituting eqs.(3.11) and (3.13) into eq.(3.17), we obtain Ψ_b. Then using the result together with eq.(3.14) we calculate eq.(3.16b) to obtain

$$n_f(T) \simeq \begin{cases} 1 - a(T)\varphi(T) \quad (\text{at } T << E_0) , & (3.18a) \\ 1 - b(T)/(N+\Phi(T)) \quad (\text{at } T >> E_0) , & (3.18b) \end{cases}$$

with

$$b(T) \equiv \frac{1}{\pi} \int_{-\infty}^{\infty} d\omega \ \Delta_0 f(\omega) /$$

$$[\{E_0(T)-\omega-\frac{\Delta_0}{\pi}\log\left|\frac{2\pi T}{E_0(T)}\right|-\frac{\Delta_0}{\pi}\mathrm{Re}\Psi(\frac{1}{2}+i\frac{\omega}{2\pi T})\}^2+\{\Delta_0 f(\omega)\}^2]e^{\beta\omega} , \quad (3.19)$$

where $\varphi(T)$ is defined by eq.(2.36). Here we note that the number of the f-electron given in eq.(3.18) is not strongly temperature-dependent, while its components, the coherent part $\Delta n_f^{(0)}$ and the incoherent part n_f^0 are rather strongly dependent on the temperature. Substituting eq.(3.14) to eq.(2.46a) we obtain n_f^0,

$$n_f^0 \simeq \begin{cases} 0 \quad (\text{at } T << T_0) , & (3.20a) \\ N^{(1-T_0/T)}\varphi(T) \quad (\text{at } T_0 \lesssim T << E_0) , & (3.20b) \\ N/(N+\Phi(T)) \quad (\text{at } T >> E_0) , & (3.20c) \end{cases}$$

where T_0 is the coherence temperature defined by eq.(2.38). The temperature dependence of n_f^0 is important to that of the magnetic

susceptibility (see Sec. 3.2).

The lowest order contribution to the average number of the c-electron in the 1/N-expansion is obtained by using eqs.(3.3) and (3.4) as

$$n_c(T) = \int_{-\infty}^{\infty} d\omega \; N\tilde{\rho}_m(\omega) f(\omega)$$

$$\propto \begin{cases} N\rho_m^0 |E^-_{min.}(T)| & (\text{at } T << E_0) \qquad (3.21a) \\ N\rho_m^0 |D+\mu(T)| & (\text{at } T >> E_0) \; . \qquad (3.21b) \end{cases}$$

3.2 Magnetic susceptibility

In order to calculate the magnetic susceptibility χ_m, we include the Zeeman energy and replace ε_{k_m} and ε_f in eqs.(2.2) and (2.3) respectively by

$$\tilde{\varepsilon}_{k_m} \equiv \varepsilon_{k_m} - mh_c \; , \text{ with } h_c \equiv g_c \mu_B H \; , \qquad (3.22a)$$

and

$$\tilde{\varepsilon}_{fm} \equiv \varepsilon_f - mh_f \; , \text{ with } h_f \equiv g_f \mu_B H \; . \qquad (3.22b)$$

Correspondingly we also replace ε_{k_m} and ε_f by $\tilde{\varepsilon}_{k_m}$ and $\tilde{\varepsilon}_{fm}$ in eqs.(2.10),(2.12),(2.14),(2.16),(2.18),(2.19),(2.21) and (2.23). Then the magnetization of the c-electron $\langle m_c \rangle$ and that of the f-electron $\langle m_f \rangle$ are given by

$$\langle m_c \rangle \equiv g_c \mu_B \sum_{m=-J}^{J} m \frac{1}{N_L} \sum_{k_m} [T \sum_{\omega_n} G_{k_m}(i\omega_n) e^{i\omega_n 0_+}] , \qquad (3.23a)$$

$$\langle m_f \rangle \equiv g_f \mu_B \sum_{m=-J}^{J} m \lim_{\lambda_i \to \infty} [\langle \hat{n}_{fim} \rangle_\lambda / \langle \hat{Q}_i \rangle_\lambda] . \qquad (3.23b)$$

Differentiating eq.(3.23) with respect to the magnetic field H we obtain the lowest order contribution to χ_m in the 1/N-expansion as

$$\chi_m = \frac{\partial \langle m_c \rangle}{\partial H} + \frac{\partial \langle m_f \rangle}{\partial H} \equiv \chi_m^{cc} + \chi_m^{cf} + \chi_m^{fc} + \chi_m^{ff} , \qquad (3.24)$$

where

$$\chi_m^{cc} \equiv g_c \mu_B \left(\frac{\partial \langle m_c \rangle}{\partial h_c}\right)_{h_f}$$

$$= (g_c \mu_B)^2 \frac{1}{N_L} \sum_{mk_m} m^2 [-T \sum_{\omega_m} \{G_{k_m}(i\omega_n)\}^2] , \qquad (3.25a)$$

$$\chi_m^{cf} \equiv g_f \mu_B \left(\frac{\partial \langle m_c \rangle}{\partial h_f}\right)_{h_c}$$

$$= (g_c \mu_B)(g_f \mu_B) \frac{1}{N_L} \sum_{mk_m} m^2 [T \sum_{\omega_n} \{G_{k_m}(i\omega_n)\}^2 \frac{d}{d(i\omega_n)} \Sigma_{k_m}(i\omega_n)] ,$$

(3.25b)

$$\chi_m^{fc} \equiv g_c\mu_B\left(\frac{\partial\langle m_f\rangle}{\partial h_c}\right)_{h_f} = \chi_m^{cf} \ , \tag{3.25c}$$

$$\chi_m^{ff} \equiv g_f\mu_B\left(\frac{\partial\langle m_f\rangle}{\partial h_f}\right)_{h_c}$$

$$= (g_f\mu_B)^2 \sum_m m^2 \{ \lim_{\lambda_i\to\infty} [-T \sum_{\omega_n} \{F_m^0(i\omega_n-\lambda_i)\}^2/\langle\hat{Q}_i\rangle_\lambda]$$

$$+ \frac{1}{N_L}\sum_{k_m} [-T \sum_{\omega_m} G_{k_m}(i\omega_n)\frac{d^2}{d(i\omega_n)^2}\Sigma_{k_m}(i\omega_n)]$$

$$+ \frac{1}{N_L}\sum_{k_m} [-T \sum_{\omega_m} \{G_{k_m}(i\omega_n)\frac{d}{d(i\omega_n)}\Sigma_{k_m}(i\omega_n)\}^2]\} \ . \tag{3.25d}$$

If we assume that f- and c-electrons have the same g-value, i.e., $g_f=g_c=g$, then eq.(3.24) is rewritten as

$$\chi_m = \frac{1}{3}(g\mu_B)^2 J(J+1)[\bar{\chi}_m^0 + \Delta\bar{\chi}_m^{(0)}] \ , \tag{3.26}$$

where the normalized susceptibilities are defined by

$$\bar{\chi}_m^0 \equiv N \lim_{\lambda_i\to\infty} [-T \sum_{\omega_n} \{F_m^0(i\omega_n-\lambda_i)\}^2/\langle\hat{Q}_i\rangle_\lambda] \ , \tag{3.27}$$

$$\Delta\bar{\chi}_m^{(0)} \equiv \frac{1}{N_L}\sum_{mk_m} [T \sum_{\omega_n} \frac{d^2}{d(i\omega_n)^2} \log[G_{k_m}(i\omega_n)]^{-1}] \ . \tag{3.28}$$

In above, $\bar{\chi}_m^0$ is due to the bare f-electron and $\Delta\bar{\chi}_m^{(0)}$ is due to the lowest order contribution in the 1/N-expansion. Performing the analytic continuation and/or the k_m-summation in eqs.(3.27) and (3.28) yields

$$\bar{\chi}_m^0 = \frac{n_f^0(T)}{T} , \tag{3.29}$$

and

$$\Delta\bar{\chi}_m^{(0)} = \Delta\bar{\chi}_m^{(a)} + \Delta\bar{\chi}_m^{(b)} , \tag{3.30}$$

with

$$\Delta\bar{\chi}_m^{(a)} \equiv \int_{-\infty}^{\infty} d\omega(-\frac{df(\omega)}{d\omega})(1-\frac{d}{d\omega}Re\Sigma(\omega))N\tilde{\rho}_m(\omega) , \tag{3.31a}$$

$$\Delta\bar{\chi}_m^{(b)} \equiv \frac{N\rho_m^0}{2\pi}\int_{-\infty}^{\infty} d\omega(-\frac{df(\omega)}{d\omega})(\frac{d}{d\omega}Im\Sigma(\omega))\log[\frac{(\omega+\mu-Re\Sigma(\omega)+D)^2+(Im\Sigma(\omega))^2}{(\omega+\mu-Re\Sigma(\omega)-D)^2+(Im\Sigma(\omega))^2}] , \tag{3.31b}$$

where n_f^0 is the number of the incoherent and localized part of the f-electron defined by eq.(2.46a). Substituting eq.(3.20) into eq.(3.29) we obtain

$$\bar{\chi}_m^0(T) \propto \begin{cases} 0 & (\text{at } T << T_0) , \quad (3.32a) \\ N^{(1-T_0/T)}\varphi(T)/T & (\text{at } T_0 \lesssim T << E_0) , \quad (3.32b) \end{cases}$$

$$\left\{ \frac{N}{N+\Phi(T)} \frac{1}{T} \qquad (\text{at } T >> E_0) \ . \right. \tag{3.32c}$$

Substituting eqs.(2.35b) and (3.4a) into eq.(3.31a) yields

$$\Delta\bar{\chi}_m^{(a)}(T) \simeq \begin{cases} N\rho_m^0 \left(1 + \frac{a(T)\varphi(T)V}{E_0(T)^2}\right)^2 & (\text{at } T << E_0) \ , \qquad (3.33a) \\ N\rho_m^0 & (\text{at } T >> E_0). \qquad (3.33b) \end{cases}$$

We note that $\Delta\bar{\chi}_m^{(a)}$ includes the terms due to the c-electron given in eqs.(3.25a)~(3.25c), while the enhancement factor $a(T)\varphi(T)V^2/E_0(T)^2 >> 1$ at $T \lesssim T_0$ in eq.(3.33a) comes from the contribution only of the f-electron χ_m^{ff} in eq.(3.25d). We find $\Delta\bar{\chi}_m^{(b)}$ is negative but negligible compared with $\Delta\bar{\chi}_m^{(a)}$ at $T \lesssim T_0$:

$$|\Delta\bar{\chi}_m^{(b)}(T)| \propto e^{-\beta E_0(T)} << \Delta\bar{\chi}_m^{(a)}(T) \ (\text{at } T \lesssim T_0) \ . \tag{3.34}$$

The mass enhancement factor, $1+aV^2/E_0^2$ in χ_m at T=0, (see Sec. 3.4), is plotted as a function of n in Fig.7.

Eqs.(3.32)~(3.34) show that χ_m is strongly enhanced at $T \lesssim T_0$, while it decreases with increasing temperature at $T \gtrsim T_0$ and has a rather sharp peak at $T \simeq T_0$. This result is essentially the same as that obtained for the impurity Anderson model[16] except for the energy scale, the Kondo temperature T_k in the latter while E_0 in the present case. However, as shown in Sec. 4, the feature at $T \lesssim T_0$ in the realistic Anderson lattice with N=6 is more complicated.

3.3 Density of states for the f-electron

From the expression for the f-electron Green's function eq.(2.42a), the lowest order contribution to the density of states for the f-electron in the 1/N-expansion is given by

$$\tilde{\rho}_m^f(\omega) \equiv \frac{1}{N_L} \sum_{k_m} [-\frac{1}{\pi} \mathrm{Im} G^f_{k_m}(\omega + i0_+)]$$

$$\simeq \tilde{\rho}_m^{f(a)}(\omega) + \tilde{\rho}_m^{f(b)}(\omega) \ ,$$

with

$$\tilde{\rho}_m^{f(a)}(\omega) \equiv \tilde{\rho}_m(\omega)[(\mathrm{Re}\Sigma(\omega)/V)]^2 \ , \tag{3.35a}$$

$$\tilde{\rho}_m^{f(b)}(\omega) \equiv \rho_m^0 \frac{1}{\pi}(\frac{-\mathrm{Im}\Sigma(\omega)}{V^2})\{2D - \mathrm{Re}\Sigma(\omega) \log[\frac{(\omega+\mu-\mathrm{Re}\Sigma(\omega)-D)^2+(\mathrm{Im}\Sigma(\omega))^2}{(\omega+\mu-\mathrm{Re}\Sigma(\omega)+D)^2+(\mathrm{Im}\Sigma(\omega))^2}]\}$$

$$- \tilde{\rho}_m(\omega)[\mathrm{Im}\Sigma(\omega)/V]^2 \ . \tag{3.35b}$$

Substituting eq.(2.35) into eq.(3.35) we obtain at $T \lesssim T_0$

$$\tilde{\rho}_m^{f(a)}(0) \simeq \tilde{\rho}_m(0)[\frac{a(T)\varphi(T)V}{E_0(T)}]^2 \ , \tag{3.36a}$$

$$\tilde{\rho}_m^{f(b)}(0) \propto e^{-\beta E_0(T)} << \tilde{\rho}_m^{f(a)}(0) \ . \tag{3.36b}$$

Since $(a(T)\varphi(T)V/E_0(T))^2 >> 1$ at $T \lesssim T_0$, the density of states for the f-electron at the Fermi level $\tilde{\rho}_m^f(0)$ is considerably larger than that for the c-electron $\tilde{\rho}_m(0) \simeq \rho_m^0$. In Fig.7, $\tilde{\rho}^f(0) \equiv N\tilde{\rho}_m^f(0)$ and $\tilde{\rho}(0) \equiv N\tilde{\rho}_m(0)$ at T=0 are plotted as functions of n. We find, from eq.(3.10), that the satulated value of $\tilde{\rho}^f(0)$ for $E_0 << |\bar{E}_{min.}|$ and $a << 1$ at $T << T_0$ is given by π/Δ_0 ($\simeq 44.4$ for D=1 and V=0.15) which is independent of ε_f^0. While, at $T >> E_0$, we find that $\tilde{\rho}_m^{f(a)}(\omega) << \rho_m^0$ and $\tilde{\rho}_m^{f(b)}(\omega)$ contributes to the density of states for $\omega \simeq \varepsilon_f$, i.e., the f-electron almost localizes near the atomic f-level.

Here we note that, at $T \lesssim T_0$, $\tilde{\rho}_m^{f(a)}(\omega)$ contributes to the density of states for $|\omega| \lesssim E_0$, while the density of states for $|\omega| \gtrsim E_0$ comes from the higher order corrections in the 1/N-expansion as has been studied in the impurity Anderson model[19]. Thus integration over ω of $\tilde{\rho}_m^{f(a)}(\omega)$ in eq.(3.35a) multiplied by $f(\omega)$ gives the number of the f-electron around the Fermi level, $|\omega| \lesssim E_0$, which may be identified with the number of the itinerant f-electron:

$$n_f^{itin.}(T) \equiv \int_{-\infty}^{\infty} d\omega \, N\tilde{\rho}_m^{f(a)}(\omega) f(\omega)$$

$$\simeq a(T)\varphi(T) n_f(T) \ , \quad \text{at } T \lesssim T_0 \ . \tag{3.37}$$

Since $a(T)\varphi(T) << 1$, $n_f^{itin.}(T)$ is much smaller than the total number of the f-electrons $n_f(T)$ given by eq.(3.18a). Hence, at $T \lesssim T_0$, most of the f-electrons are coherent but localized (note

that the localized and incoherent part $n_f^0=0$ at $T<<T_0$ as shown in eq.(3.20a)) which gives the strongly enhanced Pauli paramagnetic susceptibility given in eq.(3.33a).

3.4 Quasi-particles

As mentioned in Sec. 2 energies of the quasi-particles, $z=E_k-i\Gamma_k$, are given by the poles of the c- or the itinerant f-electron Green's function:

$$z+\mu-\xi_k-\mathrm{Re}\Sigma(z) = 0 \ . \tag{3.38}$$

If we assume the linear dispersion for the bare c-electron band, i.e., $\xi_k \equiv D(k/\pi-1)$ for $0 \leq k < 2\pi$, the Fermi wave vector k_F or the phase volume enclosed by the Fermi surface V_{phase} is determined by

$$V_{phase} \equiv k_F/\pi = [D+\mu-\mathrm{Re}\Sigma(0)]/D \ . \tag{3.39}$$

Using eqs.(2.35b), (3.10), (3.18) and (3.21) in eq.(3.39), we obtain relations to the lowest order contribution in the 1/N-expansion as

$$V_{phase} \simeq \begin{cases} n_c + n_f & (\text{at } T << T_0) \ , \quad (3.40a) \\ n_c+n_f-(1-\varphi(T)) & (\text{at } T_0 \lesssim T << E_0) \ , \quad (3.40b) \\ n_c(T) - \mathrm{Re}\Sigma(0)/D & (\text{at } T >> E_0) \ . \quad (3.40c) \end{cases}$$

This result shows that the Fermi surface is determined by sum of the c- and f-electrons at $T \ll T_0$ as shown in Sec. 2 more generally as the Luttinger sum rule, while it is determined almost only by the c-electrons at $T \gg E_0$, and V_{phase} decreases rapidly with increasing temperature at $T_0 \lesssim T \ll E_0$.

The mass enhancement factor at the Fermi level is given by

$$\frac{m^*}{m} = 1 - \frac{d}{d\omega} \mathrm{Re}\Sigma(\omega)\Big|_{\omega=0} \cdot \tag{3.41}$$

Substituting eq.(2.35b) with eq.(2.37) to eq.(3.41) yields to the lowest order contribution in the 1/N-expansion

$$\frac{m^*}{m} \simeq \begin{cases} 1 + \dfrac{a(T)\varphi(T)V^2}{E_0(T)^2} & (\text{at } T \ll E_0) , \qquad (3.42a) \\ \\ 1 & (\text{at } T \gg E_0) . \qquad (3.42b) \end{cases}$$

m^*/m is much enhanced at $T \lesssim T_0$ by the factor $a(T)\varphi(T)V^2/E_0(T)^2 \gg 1$ which also enhances χ_m at $T \lesssim T_0$ as shown in eq.(3.33), while at $T \gg E_0$ it is almost unity and decreases rapidly with increasing temperature at $T_0 \lesssim T \ll E_0$. In Fig.6, m^*/m at T=0 is plotted as a function of n.

3.5 Life time of the conduction electron

The inverse life time $1/2\tau$ of the c-electron is given by the imaginary part of the self-energy at the Fermi level:

$$\frac{1}{2\tau} = - \mathrm{Im}\Sigma(\omega+i0_+)\Big|_{\omega=0} \ . \qquad (3.43)$$

Using eqs.(3.11),(3.13) and (3.14) in eq.(2.24) we obtain

$$\frac{1}{2\tau} \simeq \begin{cases} 0 & (\text{at } T << T_0) \ , \qquad (3.44a) \\ \dfrac{\pi D}{N} N^{(1-T_0/T)} \varphi(T) \left[\left\{ \dfrac{\pi E_0(T)}{\Delta_0} + \log \left| \dfrac{2\gamma E_0(T)}{\pi T} \right| \right\}^2 + \left(\dfrac{\pi}{2}\right)^2 \right]^{-1} & \\ \qquad (\text{at } T_0 \lesssim T << E_0) \ , \qquad (3.44b) \\ \dfrac{\pi D}{N+\Phi(T)} \left[\left\{ \dfrac{\pi E_0(T)}{\Delta_0} + \log \left| \dfrac{2\gamma E_0(T)}{\pi T} \right| \right\}^2 + \left(\dfrac{\pi}{2}\right)^2 \right]^{-1} & \\ \qquad (\text{at } T >> E_0) \ , \qquad (3.45c) \end{cases}$$

where γ is the Euler constant. With increasing temperature $1/2\tau$ increases at $T<<E_0$, while it decreases at $T>>E_0$. The peak of $1/2\tau$ appears at the intermediate temperature. We need to do numerical calculations to determine the overall temperature dependence of $1/2\tau$, which will be done in Sec. 4. Here we note that we need to include higher order corrections in the 1/N-expansion to obtain the Fermi liquid like life time proportional to ω^2 and T^2 in 3-dimension at $T<<T_0$ which has been studied in Ref.[18] and more extensively in Ref.[20]. We also note that the effect of the dimensionality appears only through the higher order corrections in the 1/N-expansion.

4. Numerical Results over the Whole Temperature Range

The numerical calculation is performed to solve the integral equations (2.24)~(2.30) over the whole temperature range. All the functions of ω involved in the calculation are defined on the discrete mesh points of ω separated by small increments, $\Delta\omega=(\Delta\omega)_{max.}-((\Delta\omega)_{max.}-(\Delta\omega)_{min.})C^2/[(\omega-\omega_A)^2+C^2]$, where ω_A is the frequency of the peak of the spectral functions of the slave-boson and $(\Delta\omega)_{max.}=(0.7\sim2.0)\times10^{-2}D$, $(\Delta\omega)_{min.}=(0.1\sim3.0)\times10^{-5}D$, $C=(0.04\sim0.12)D$. The total numbers of the mesh points in the calculations are $N_{mesh}=167\sim988$.

For all the calculations in this section, the parameters are chosen as follows: the spin-orbital degeneracy N=6, the bare density of states for the c-electron $\rho_m^0(\xi)=(6D)^{-1}$ for $-D<\xi<D$ (see Sec. 3), the hybridization energy V=0.15D, the bare atomic level of the f-electron $\varepsilon_f^0=-0.15D$ measured relative to the center of the bare c-band and the total number of the electrons per unit cell $n=n_c+n_f=1.9$. As the result, we obtain at T=0 the binding energy $E_0=21.6\times10^{-4}D$, the residue a=0.0877, the number of the f-electron $n_f=0.912$, the mass enhancement factor at the Fermi level $m^*/m=425$ and the renormalized density of states for the f-electron at the Fermi level $\tilde{\rho}^f(0)=37.2$ as shown in Sec. 3 (see Figs.6~8).

At higher temperature $T\gtrsim3E_0$, the solutions are almost independent of the numbers of the mesh points for $N_{mesh}\gtrsim200$. On the other hand, as the temperature becomes lower, the peak of the spectral function of the slave-boson becomes sharper. As a result, convergence of the numerical calculations becomes very poor due to the discreteness of the mesh points. In order to

avoid such difficulty we divide the spectral function of the slave-boson into two parts: the resonance spectrum given by the function (3.11a) treated analytically and the remaining continuous spectrum treated numerically on the mesh points.

Fig.9 shows the N_{mesh} dependence of the binding energy $E_0(T)$ of the resonance level calculated by the definition eq.(2.32). For the calculation at lower temperatures, we must use larger values of N_{mesh} in order to obtain the convergent solutions. For example, for the calculations with N_{mesh}=988, the lowest temperature where we obtain the convergent solution is about $T=0.15E_0$.

In order to obtain the convergent solutions at further lower temperature $T\lesssim 0.15E_0$, the resonance spectrum is approximated by the delta functions, i.e., $a(T)\delta(\omega-E_0(T))$, and furthermore the continuous spectrum is approximated by the analytic function of ω, eq.(3.11b), instead of using the discrete mesh points. The results of this approximation agree very well with those of the calculations using the discrete mesh points at $T\lesssim 0.2E_0$ as shown in Fig.9. Here we note that the sum rules for the spectral functions (their integrations over ω must be unity) are always checked to hold to the accuracy within 0.1%.

In Fig.10, the spectral function of the slave-boson is plotted as a function of ω. At higher temperature $T=1.39E_0$, it shows a single broad peak at the resonance level, $\omega=E_0(T)(\simeq 2.1E_0)$. On the other hand, at lower temperature $T=0.46E_0$, it shows a sharp resonance peak at $\omega=E_0(T)(\simeq 1.5E_0)$ together with two continua away both sides of the resonance peak. The separation of the continua is caused by the hybridization gap

of the renormalized bands, as clearly seen in eq.(3.11b) together with eqs.(3.2) and (3.4a). The lower continuum is from the lower renormalized band for $E^{-}_{min.}<\omega<E^{-}_{max.}$ and the upper continuum is from the upper one for $E^{+}_{min.}<\omega<E^{+}_{max.}$. At higher temperature, when the hybridization gap vanishes, the resonance peak and the continua are combined to give a single broad peak. Here we note that the integrated intensity of the resonance peak, i.e., the residue of the resonance state, eq.(2.33), for $T=0.46E_0$ is even larger than that for $T=1.39E_0$ as will be shown in Fig.12.

Using eqs.(2.32), (2.33) and (3.12), we calculate the binding energy $E_0(T)$, the residue $a(T)$ and the half width $\Gamma(T)$ of the resonance level. They are plotted as functions of T in Figs.11~13. In Fig.11, $E_0(T)$ shows a minimum at $T\simeq 0.16E_0$ and two peaks: a small peak at $t\simeq 0.03E_0$ and a broad one at $T\simeq 1.8E_0$; $E_0(T=1.8E_0)\simeq 2.2E_0$. It monotonously decreases as a function of T at $T\gtrsim 1.8E_0$ and becomes negative at $T\gtrsim 3.5E_0$. The minimum structure of $E_0(T)$ at $T\simeq 0.16E_0$ leads to peak structures of quantities as shown later.

In Fig.12, $a(T)$ shows a broad peak at $T\simeq 0.5E_0$ and two minima: a small minimum at $T\simeq 0.08E_0$ and a rather large one at $T\simeq 1.3E_0$. $a(T)$ is not very well defined at $T\gtrsim 1.2E_0$, because the resonance peak overlaps with the continua.

Fig.13 shows that $\Gamma(T)$ decreases rapidly with decreasing T at $T\lesssim 1.2E_0$; this is a consequence of the development of the hybridization gap shown in Fig.17.

In Fig.14, the imaginary part and the real part of the self-energy of the c-electron are plotted as functions of ω. From

eq.(2.24), the shape of the imaginary part reflects that of the spectral function of the slave-boson (see Fig.10).

By using eq.(3.38), energies of quasi-particles, $z_k=E_k-i\Gamma_k$, are calculated. E_k (the solid line) and $E_k\pm\Gamma_k$ (the broken line) are plotted as functions of k in Fig.15. At lower temperature $T=0.46E_0$, they show the renormalized band structure with hybridization gap, while, at higher temperature $T=1.39E_0$, they show the renormalized band structure with a pseudo gap (see Fig.16).

The renormalized density of states for the c-electron and that for the f-electron are defined by $\tilde{\rho}^c(\omega)\equiv N\tilde{\rho}(\omega)$ with eq.(3.3) and $\tilde{\rho}^f(\omega)\equiv N\tilde{\rho}^f_m(\omega)$ with eq.(3.35), respectively. We plot them as functions of ω in Fig.16. At lower temperature $T=0.46E_0$, they show the hybridization gap structure, while, at higher temperature $T=1.39E_0$, they show a pseudo gap structure. Here we note that the density of states inside the hybridization gap is extremely small but finite at finite temperature and is zero only at T=0.

In order to determine the magnitude of the hybridization gap, we use the condition, $\tilde{\rho}^c(\omega)<(100D)^{-1}$ for ω inside the gap. The temperature dependence of the hybridization gap thus obtained is plotted in Fig.17, where, for the sake of the contrast, we also plot the hybridization gap calculated by the slave-boson mean field theory (SBMFT) originally developed by Coleman[14] and Millis and Lee[15]. A distinct contrast between the present result and that of SBMFT is evident at $T\gtrsim 0.16E_0$.

As shown in the previous sections, in the present theory of the 1/N-expansion, the resonance part in the slave-boson spectral

function contributes most dominantly to determine the properties of the heavy Fermi liquid state at lower temperature $T<<T_0$, while the continuum in that contributes most dominantly to determine those at higher temperature $T\gtrsim T_0$. On the other hand, in SBMFT, the contributions from the continuum is entirely neglected over the whole temperature range. Through these discussions together with the results in Fig.17, we may define the coherence temperature as $T_0 \equiv 0.16E_0$ in the present model with N=6, although T_0 in the large N limit is defined by eq.(2.38). In the present model, the hybridization gap deceases rapidly with increasing T at $T\gtrsim T_0$ and vanishes finally at a certain temperature T_{gap}, which is given by $T_{gap} \equiv 1.2E_0$ in the present model as seen in Fig.17. At $T\gtrsim T_{gap}$, it changes to the pseudo gap (see Fig.16). On the other hand, in SBMFT, the hybridization gap vanishes at the transition temperature $T_c \simeq 55.6E_0$ when the order parameter in SBMFT, i.e., the anomalous average of the slave-boson $\langle\hat{b}\rangle$, vanishes. Here we again emphasize that these distinct contrasts at $T\gtrsim T_0$ between the two types of the theories are caused by the contributions due to the continuum in the slave-boson spectral function; these contributions are rigorously treated in the present theory within the lowest order contributions in the 1/N-expansion, while they are completely neglected in SBMFT.

In Fig.18, the renormalized density of states at the Fermi level for the f-electron $\tilde{\rho}^f(0)$ and that for the c-electron $\tilde{\rho}^c(0)$ are plotted as functions of T. $\tilde{\rho}^f(0)$ is considerably larger than $\tilde{\rho}^c(0)(\simeq 1)$ at $T\lesssim T_0$, deceases rapidly with increasing T at $T_0 \lesssim T \lesssim T_{gap}$ and has a rather sharp peak at $T \simeq T_0$. At $T\gtrsim T_{gap}$, it

decreases gradually with increasing T to become much less than unity. $\tilde{\rho}^c(0)$ is almost independent of T and about unity. It shows a small minimum at $T\simeq 3.5E_0$; this is due to the pseudo gap structure at $\omega\simeq E_0(T)\simeq 0$ (see Figs.16 and 11).

Fig.19 shows the temperature dependence of the mass enhancement factor m^*/m at the Fermi level defined by eq.(3.41). m^*/m is much larger than unity at $T\lesssim T_0$, while it decreases rapidly with increasing T at $T_0\lesssim T\lesssim T_{gap}$ and shows a rather sharp peak at $T\simeq T_0$. It decreases gradually with increasing T at $T_{gap}\lesssim T\lesssim 6E_0$ to $m^*/m\simeq -4.2$, increases at $6E_0\lesssim T\lesssim 60E_0$ to $m^*/m\simeq 1.4$ and again decreases at $T\gtrsim 60E_0$ to $m^*/m\simeq 1$. Here we note that, at $3.5E_0\lesssim T\lesssim 25E_0$, m^*/m is smaller than unity and may be negative; this temperature dependence will be discussed later.

Using eq.(3.39), we calculate the phase volume V_{phase} in the k-space enclosed by the Fermi surface. In Fig.20, V_{phase} is plotted as a function of T together with the number of the conduction electron n_c. At $T\lesssim T_0$, $V_{phase}\simeq n_c+n_f=1.9$ (the Luttinger sum rule is satisfied), while it decreases rapidly with increasing T at $T_0\lesssim T\lesssim T_{gap}$ and shows a rather sharp peak at $T\simeq T_0$. It decreases gradually with increasing T at $T_{gap}\lesssim T\lesssim 25E_0$ to $V_{phase}\simeq 0.92$ and increases at $T\gtrsim 25E_0$ together with $n_c(T)$ to $V_{phase}\simeq n_c(T)$. From eqs.(3.36a), (3.42a) and (3.39), we find that the peak structure in T-dependence of $\tilde{\rho}^f(0)$, m^*/m and V_{phase} at $T\simeq T_0$ followed by rapid increases at $T\gtrsim T_0$ as shown in Figs.18~20 are mainly due to the minimum structure in $E_0(T)$ at $T\simeq T_0$ shown in Fig.11. These structures are just a consequence of the contributions from the continuum in the slave-boson spectral function.

Fig.21 shows the temperature dependence of the number of the f-electrons, where the bare contributions n_f^0, the contribution of $O((1/N)^0)$ $\Delta n_f^{(0)}$ and the sum of the two contributions $n_f=n_f^0+\Delta n_f^{(0)}$ are calculated by using eqs.(2.46a) and (3.16b). As mentioned in Sec. 2, n_f^0 corresponds to the localized and incoherent part of the f-electron and $\Delta n_f^{(0)}$ corresponds to the coherent part. At $T \lesssim T_0$, $n_f \simeq \Delta n_f^{(0)}$ and $n_f^0 \simeq 0$, while, with increasing T at $T \gtrsim T_0$, n_f^0 increases and $\Delta n_f^{(0)}$ decreases and, at $T \gtrsim 180E_0$, $n_f \simeq n_f^0$ and $\Delta n_f^{(0)} \simeq 0$. A saturation of n_f^0 is seen at $T \gtrsim 40E_0$; this is due to the charge fluctuation of the localized f-electron near the atomic f-level $\varepsilon_f^0 \simeq -69.4E_0$. We note that, as shown in eq.(3.37), the number of the itinerant f-electrons staying around the Fermi level $|\omega| \lesssim E_0$ is $n_f^{itin.} \lesssim 0.1 n_f$ at $T \lesssim T_0$. Therefore, we may conclude that most of the f-electrons are localized even in the lowest temperature regime.

In Fig.22, we plot the number of the c-electrons n_c and that of the f-electrons $n_f=n_f^0+\Delta n_f^{(0)}$ calculated by using eqs.(3.21) and (3.16b), respectively, together with those calculated by SBMFT as functions of T. Distinct contrasts between the two types of theories are again seen at $T \gtrsim T_0$. In the present theory, a saturation of n_f is observed at $T \simeq 6.5E_0$. On the other hand, in SBMFT, n_f increases monotonously with increasing T and $n_f=1$ at $T \geq T_c \simeq 55.6E_0$. In SBMFT, all of the f-electrons stay in the hybridized band and there is no localized f-electrons at $T<T_c$. This is quite a contrast to the present theory as mentioned above.

Fig.23 shows the temperature dependence of the normalized

susceptibilities, the bare contribution $\bar{\chi}_m^0$, the contribution of $O((1/N)^0)$ $\Delta\bar{\chi}_m^{(0)}$ and the sum of the two contributions $\bar{\chi}_m=\bar{\chi}_m^0+\bar{\chi}_m^{(0)}$, which are defined by eqs. (3.26)~(3.28) and calculated by using eqs. (3.29) and (3.31).

$\bar{\chi}_m^0$ in eq. (3.29) is expressed in a Curie-law like form with the effective local moment $n_f^0(T)$ which is much temperature dependent as shown in Fig.21. On the contrary, $\bar{\chi}_m^{(0)}$ in eq. (3.31a) shows an enhanced Pauli paramagnetic behavior due to the quasi-particles forming the renormalized bands. At $T\lesssim T_0$, $\bar{\chi}_m\simeq\Delta\bar{\chi}_m^{(0)}$ and decreases rapidly with increasing T, while $\bar{\chi}_m^0\simeq 0$. At $T\gtrsim T_0$, with increasing T, $\bar{\chi}_m^0$ increases rapidly to take a maximum $\bar{\chi}_m^0\simeq 165$ at $T\simeq 0.3E_0$ and then decreases gradually at $T\gtrsim 0.3E_0$ to $\bar{\chi}_m^0\simeq 0$, while $\Delta\bar{\chi}_m^{(0)}$ decreases gradually to take a minimum $\Delta\bar{\chi}_m^{(0)}\simeq -6.0$ at $T\simeq 1.6E_0$ and then increases gradually to $\Delta\bar{\chi}_m^{(0)}\simeq 0$. $\bar{\chi}_m$ shows a peak $\bar{\chi}_m\simeq 275$ at $T\simeq 0.24E_0$ and a minimum $\bar{\chi}_m\simeq 230$ at $T\simeq 0.14E_0$.

The curious minimum structure of $\bar{\chi}_m$ obtained above is understood as follows: When the number of electrons n is close to 2, the lower edge of the hybridization gap. i.e., the upper edge of the lower renormalized band $E^-_{max.}(T)$, is close to the Fermi level, i.e., $E^-_{max.}(T)\ll E_0$ at $T\lesssim T_0$. If $E^-_{max.}(T)$ is lower than T_0, the hybridization gap may give indispensable corrections to the thermodynamic properties of the heavy Fermi liquid state at $T\lesssim T_0$. A very rapid decrease of $\Delta\bar{\chi}_m^{(0)}$ shown in Fig. 23 is a consequence of these correction. Actually, as shown in Fig.17, $E^-_{max.}(T)\lesssim 0.1E_0<T_0$ in the present model with n=1.9. This rapid decrease of $\Delta\bar{\chi}_m^{(0)}$ causes a minimum structure of $\bar{\chi}_m$. We find that, as n leaves from 2, the minimum structure of $\bar{\chi}_m$ diminishes

and finally changes to a single peak structure at $T \simeq T_0$ for $n \simeq 1$.

In Fig. 24, the inverse of the normalized magnetic susceptibility $\bar{\chi}_m^{-1}$ is plotted as a function of T. At $T \gtrsim E_0$, the temperature dependence of $\bar{\chi}_m^{-1}$ is determined by almost only that of $\bar{\chi}_m^{0\ -1} = T/n_f^0$, because $\Delta\bar{\chi}_m^{(0)} << \bar{\chi}_m^0$ as shown in Fig.23.

Fig. 25 shows the temperature dependence of the inverse of the life time $1/2\tau$ of the c-electron given by eq.(3.43). It shows, with increasing T, a linear-T-like increase at $T_0 \lesssim T \lesssim T_{gap}$, a log T-like decrease at $T \gtrsim 5E_0$ and a peak $1/2\tau \simeq 0.13D$ at $T \simeq 5E_0$. As mentioned in Sec. 3.5, the Fermi liquid like life time is neglected in the present calculation as higher order corrections in the 1/N-expansion, hence $1/2\tau \simeq 0$ at $T \lesssim T_0$.

5. Conclusions

We have studied the properties of the infinite-U Anderson lattice model on the basis of the 1/N-expansion method and given a unified description over the whole temperature range unambiguously within the lowest order contributions in the 1/N-expansion. The features of the present method differing from the previous ones are:

(1) We have introduced a modified version of the N-fold degenerate Anderson lattice model, where the total degrees of freedom of the conduction electrons are divided into N subspaces in accord with the spin-orbital degeneracy of the f-electron. The density of the states in each space ρ_m^0 is assumed to be of $O(1/N)$ while the c-f hybridization V is kept to be of $O((1/N)^0)$; traditionally, V has been assumed to be of $O((1/N)^{1/2})$ while

keeping ρ_m^0 to be of $O((1/N)^0)$. The advantage of the modified version is that, even in the lowest order approximation in the expansion, we can include the inter-site coherence effect at low temperature.

(2) We have rigorously treated the local constraint throughout the calculation in each order in the expansion. As a result, the anomalous average of the slave-boson introduced in the mean-field theory vanishes over the whole temperature range and no unphysical divergence inevitable in such theory appears.

From the analytic expressions in the large N limit (Secs. 2 and 3) and the numerical results in the realistic model with N=6 (Sec. 4), we see that the present theory provide us with a unified picture of the following different temperature regimes; here it is to be stressed that the transition from one temperature range to another is *not* a distinct one, but a smooth cross over:

(1) The heavy Fermi liquid regime at $T<<T_0$

As a result of the frequent c-f mixing, at low temperatures $T \lesssim E_0 \equiv E_0(T=0)$, there appears a resonance peak with a binding energy $E_0(T)$ and a residue a(T) besides the continuous spectrum in the slave-boson spectral function. The resonance peak leads to a sharp peak at $\omega \simeq E_0(T)$ in the density of states of the f-electron. Furthermore, due to the c-f mixing, the inter-site coherence between the f-electrons and the conduction electrons sets in at $\omega \simeq E_0(T)$; it leads to the formation of the renormalized band with a hybridization gap around $\omega \simeq E_0(T)$. In this case, the continuous spectrum of the slave-boson is separated into two

parts away on the lower and upper energy sides of the resonance peak: the lower (upper) continuum is due to the lower (upper) renormalized band.

At lower temperatures $T<<T_0$ (T_0 is the coherence temperature which is defined by $T_0 \equiv 0.16E_0$ in the model with N=6 used in Sec. 4, although in the large N limit $T_0 \equiv E_0(T_0)/\log N$), the resonance part of the slave-boson contributes most dominantly in determining the properties of the heavy Fermi liquid state: the mass enhancement factor $m^*/m=1+aV^2/E_0>>1$ with $a \equiv a(T=0)$, the normalized magnetic susceptibility $\bar{\chi}_m=m^*/m >> 1$, the density of states of the f-electron at the Fermi level $\tilde{\rho}^f(0)=\rho^0(aV/E_0)^2>>1$, and the phase volume in the k-space enclosed by the Fermi surface $V_{phase}=n_c+n_f$, i.e., the Luttinger sum rule is satisfied. We have also obtained the Fermi-liquid-like life time by including the higher order corrections in the 1/N-expansion [18].

(2) The intermediate regime I at $T_0 \lesssim T \lesssim T_{gap}$

In contrast to the heavy Fermi liquid regime, at higher temperatures $T \gtrsim T_0$, the continuum (especially the upper one) of the slave-boson plays a dominant role in determining the physical properties of the system.

With increasing temperature, the magnitude of the hybridization gap decreases and, at the same time, all of m^*/m, $\bar{\chi}_m$, $\tilde{\rho}^f(0)$ and V_{phase} rapidly decrease; they show rather sharp peaks at $T \simeq T_0$ for certain values of the total electron number. The hybridization gap finally vanishes at a certain temperature T_{gap}, which is given by $T_{gap} \simeq 1.2E_0$ in the model used in Sec. 4. Note that no physical quantities are discontinuous at $T=T_{gap}$, because the density of states inside the hybridization gap is

extremely small but always finite at finite temperatures; it vanishes only at T=0.

In this regime, the inverse of the life time $1/2\tau$ is seen to increase linearly with T.

(3) The intermediate regime II at $T_{gap} \lesssim T \lesssim T_L$

At $T \gtrsim T_{gap}$, the resonance peak and the continua in the slave-boson spectral function are overlapped with each other to form a single broad peak at $\omega \simeq E_0(T)$ with a half width of $\Gamma(T)$. Accordingly, the hybridization gap turns into the pseudo gap centered at $\omega \simeq E_0(T)$ with the half width $\Gamma(T)$. $E_0(T)$ shows a broad peak as a function of T around $T=1.8E_0$ with $E_0(T=1.8E_0) \simeq 2.2E_0$, decreases monotonously with increasing T at $T \gtrsim 1.8E_0$ and finally becomes negative at $T \gtrsim 3.5E_0$. At the same time, with increasing T, $\Gamma(T)$ increases rapidly to reach a peak at $T \simeq 5E_0$ with $\Gamma(T=5E_0) \simeq 120E_0$ and decreases gradually at $T \gtrsim 5E_0$. As a consequence, the lower edge of the pseudo gap, i.e., $E_0(T)-\Gamma(T)$, becomes negative at a certain temperature T_L and further the upper edge, i.e., $E_0(T)+\Gamma(T)$, also becomes negative at a certain higher temperature T_U, where T_L and T_U are given by $T_L \simeq 2.3E_0$ and $T_U \simeq 25E_0$ respectively in the model studied in Sec. 4.

At $T_{gap} \lesssim T \lesssim T_L$, the pseudo gap is located above the Fermi level (we set it to be zero). In this regime, we can define quasi-particles with intermediate values of the mass enhancement and the phase volume: $1 \ll m^*/m \ll (m^*/m)_{T=0}$ and $n_c \lesssim V_{phase} < n_c + n_f$. With increasing T, all of m^*/m, $\bar{\chi}_m$, $\tilde{\rho}^f(0)$ and V_{phase} decrease gradually and $1/2\tau$ increases gradually.

(4) The dense Kondo regime at $T_L \lesssim T \lesssim T_U$

In this regime, the Fermi level is located inside the pseudo gap, i.e., $E_0(T)-\Gamma(T)<0$, $E_0(T)+\Gamma(T)>0$ and $\rho^c(0)$ is rather smaller than unity. Hence, we do not have the well defined quasi-particles forming the renormalized bands near the Fermi level. Actually, the mass enhancement factor defined by $m^*/m=1-\frac{d}{d\omega}\mathrm{Re}\Sigma(\omega)\Big|_{\omega=0}$ is smaller than unity and may become even negative.

$1/2\tau$ shows a peak at $T\simeq 5E_0$ and decreases logarithmically with increasing T. $\bar{\chi}_m$ and $\tilde{\rho}^f(0)$ decrease gradually as functions of T.

(5) The highest temperature regime at $T>>T_U$

In this regime, the pseudo gap is located far below the Fermi level, because $E_0(T)$ decreases monotonously with increasing T. As the result, the renormalized band is given by the bare conduction band. Correspondingly $m^*/m\simeq 1$, $\tilde{\rho}^f(0)\simeq 1$, $V_{phase}\simeq n_c$ and $1/2\tau\simeq 0$. $\bar{\chi}_m$ shows the Curie-law like behavior with the effective moment $n_f\simeq 1$, i.e., $\bar{\chi}_m\simeq n_f/T$. Thus we conclude the present model describes the incoherent regime with the bare c-electrons and the localized f-electrons at $T>>T_U$.

Acknowledgments

The author would like to express his sincere thanks to Professor Yoshihiro Kuroda and Professor Tamisufa Matsuura who kindly guided me and read the manuscript critically. He is very grateful to Professor Hisao Jichu, Professor Kazumasa Miyake, Dr. Dai S. Hirashima and Mr. Kazuo Miura who discussed with me and made useful comments on the present work. He appreciates Dr. Ken'ichi Takano, Dr. Kazuhiro Sano and Dr. Ippei Doi who advised me on the numerical calculation. He acknowledges the assistance by Mrs. Shizuko Matsuoka in typing the manuscript. He also appreciates the Fellowship of Japan Society for the Promotion of Science. This work was supported by a Grant-in-Aid for Ministry of Education, Science and Culture.

References

[1] See, for example, P. Fulde, J. Keller and G. Zwicknagle, in *Solid State Physics* (eds.), H. Ehrenrich and D. Turnbull (Academic Press, 1988) Vol.41, p.1.

[2] P. Coleman, Phys. Rev. B29 (1984) 3055.

[3] T.V. Ramakrishnan and K. Sur, Phys. Rev. B26 (1982) 1798.

[4] O. Gunnarsson and K. Schönhammer, Phys. Rev. Lett. 50 (1983) 604.

[5] N. Read and D.M. Newns, J. Phys. C16 (1983) 3273.

[6] F.C. Zhang and T.K. Lee, Phys. Rev. B28 (1983) 33.

[7] P. Coleman, Phys. Rev. B28 (1983) 5255.

[8] Y. Kuramoto, Z. Phys. B53 (1983) 33; N. Grewe, ibid. 53 (1983) 271.

[9] J.W. Rasul and A. Hewson, J. Phys. C17 (1984) 2555; ibid C17 (1984) 3337.

[10] H. Kojima, Y. Kuramoto and M. Tachiki, Z. Phys. B54 (1984) 293; Y. Kuramoto and H. Kojima, ibid. 57 (1984) 95.

[11] N.E. Bickers, D.L. Cox and J. Wilkins, Phys. Rev. Lett. 54 (1985) 230.

[12] C.-I. Kim, Y. Kuramoto and T. Kasuya, Solid State Commun. 62 (1987) 627; J. Phys. Soc. Jpn. 59 (1990) 2414.

[13] A. Auerbach and K. Levin, Phys. Rev. Lett. 57 (1986) 877.

[14] P. Coleman, Phys. Rev. B35 (1987) 5072.

[15] A.J. Millis and P.A. Lee, Phys. Rev. B35 (1987) 3394.

[16] B. Jin and Y. Kuroda, J. Phys. Soc. Jpn. 57 (1988) 1687.

[17] Y. Ōno, T. Matsuura and Y. Kuroda, Physica C 159 (1989) 878.

[18] Y. Kuroda, Y. Ōno, T. Matsuura and H. Jichu, in *Strong Correlation and Superconductivity* (eds.), H. Fukuyama, S. Maekawa and A.P. Malozemoff (Springer, Berlin, Heidelberg, 1989) p.167.

[19] B. Jin, T. Matsuura and K. Kuroda, to be published in J. Phys. Soc. Jpn. 60, No.2 (1991).

[20] K. Miura, private communication.

[21] J.M. Luttinger, Phys. Rev. 119 (1960) 1153.

Figure Captions

Fig.1 Diagrammatic description of the Dyson equations for the single particle Green's functions. The thin solid, wavy and dashed lines denote the bare c-electron, slave-boson and pseudo fermion Green's functions. The thick lines denote the corresponding renormalized Green's functions of the lowest order in the 1/N-expansion.

Fig.2 Diagrams contributing to the c-electron Green's function G_{k_m}. (a) Zeroth order terms in power of 1/N; they have no k'_m-summation because of i,j-summation and the translational invariance. (b) Higher order corrections in power of 1/N; they have more than one k'_m-summations, each of which yields an additional factor of O(1/N).

Fig.3 (a) A diagram of O(N) contributing to $\Sigma_m \langle \hat{n}_{fim} \rangle_\lambda$, (b) that of $O((1/N)^0)$ and (c) a diagram of $O((1/N)^0)$ contributing to $\langle \hat{n}_{bi} \rangle_\lambda$.

Fig.4 Diagrams of $O((1/N)^0)$ contributing to the f-electron Green's function $G^{f,\lambda}_{ijm}$.

Fig.5 Schematic structure of the renormalized bands $E^{\pm}_k$. Fermi level is set to be zero, E_0 is the binding energy and k_F is the Fermi wave vector. $-D-\mu$ and $D-\mu$ are the lower and upper band edges of the bare conduction electron band ε_k. $E^{\pm}_{min.}$ and $E^{\pm}_{max.}$ are those of the renormalized bands.

Fig.6 (a) The binding energy E_0 and (b) the residue a of the resonance state at T=0 as functions of the total number of electrons per unit cell $n=n_c+n_f$. D is a half width of the bare conduction electron band, V is the c-f

hybridization energy and ε_f^0 is the bare atomic f-level which is measured relative to the center of the bare c-electron band.

Fig.7 The mass enhancement factor at the Fermi level at T=0 $m^*/m=1+aV^2/E_0$ as a function of the total number of electrons per unit cell $n=n_c+n_f$ (see the text).

Fig.8 The density of states for the f-electron $\tilde{\rho}^f(0)$ at the Fermi level at T=0 and that for the c-electron $\tilde{\rho}^c(0)=1/D$ as functions of the total number of electrons per unit cell $n=n_c+n_f$.

Fig.9 The dependence of the binding energy $E_0(T)$ on the total number of the mesh points N_{mesh}, on which the energy dependence of the spectral functions is defined in the calculation in the present study at several low temperatures. The low temperature approximation is explained in the text.

Fig.10 The spectral functions of the slave-boson near the atomic f-level as functions of energy ω at temperatures $T/E_0=0.46$ and 1.39. The energy ω is measured in units of $E_0(T=0)$ and relative to the atomic f-level ε_f.

Fig.11 Temperature dependence of the binding energy $E_0(T)$ of the resonance level of the slave-boson.

Fig.12 Temperature dependence of the residue a(T) of the resonance level of the slave-boson. It is not very well defined at $T \gtrsim 1.2E_0$ because the resonance peak overlaps with the continuum.

Fig.13 Temperature dependence of the half width $\Gamma(T)$ of the resonance level of the slave-boson.

Fig.14 The imaginary parts (a) and the real parts (b) of the self energy of the conduction electron near the Fermi level as functions of energy ω at temperatures $T/E_0=0.46$ and 1.39. The chemical potential is set to be zero at each temperature.

Fig.15 The real parts E_k and the imaginary parts Γ_k of energies of the quasi-particles as functions of the wave number k ($0<k<2\pi$) at temperatures $T/E_0=0.46$ and 1.39. The solid line denotes E_k and the broken lines denote $E_k \pm \Gamma_k$. The chemical potential is set to be zero at each temperature.

Fig.16 The renormalized density of states for the conduction electron $\tilde{\rho}^c(\omega)$ (a) and that for the f-electron $\tilde{\rho}^f(\omega)$ (b) near the Fermi level as functions of energy ω at temperatures $T/E_0=0.46$ and 1.39. The chemical potential is set to be zero at each temperature.

Fig.17 Temperature dependence of the hybridization gap. The solid lines denote the results of the present study and the broken lines denote the results of the slave-boson mean field theory (Refs.[14,15]). A distinct contrast between two theories is seen above the coherence temperature $T_0 \equiv 0.16E_0$. The hybridization gap vanishes at $T \simeq T_{gap} \equiv 1.2E_0$ in the present theory.

Fig.18 Temperature dependence of the renormalized density of states at the Fermi level for the f-electron $\tilde{\rho}^f(0)$ (solid line) and that for the conduction electron $\tilde{\rho}^c(0)$ (broken line). $\tilde{\rho}^f(0)$ shows a rather sharp peak at the coherence temperature $T_0=0.16E_0$; $(\tilde{\rho}^f(0))_{T=T} \simeq 1.10(\tilde{\rho}^f(0))_{T=0}$ with

0 $(\tilde{\rho}^f(0))_{T=0}=(aV/E_0)^2\simeq 37.2$.

Fig.19 Temperature dependence of the mass enhancement factor m^*/m at the Fermi level. It shows a rather sharp peak at the coherence temperature $T_0=0.16E_0$; $(m^*/m)_{T=T_0}\simeq 1.11(m^*/m)_{T=0}$ with $(m^*/m)_{T=0}=1+aV^2/E_0^2\simeq 425$.

Fig.20 Temperature dependence of the phase volume V_{phase} in the k-space enclosed by the Fermi surface, and that of the number of the conduction electrons n_c. V_{phase} shows a rather sharp peak at the coherence temperature $T_0=0.16E_0$; $(V_{phase})_{T=T_0}\simeq 1.03(V_{phase})_{T=0}$ with $(V_{phase})_{T=0}=n_c+n_f=1.9$.

Fig.21 Temperature dependence of the number of the f-electrons. The short dashed line denotes the bare contribution n_f^0, the long dashed line denotes the contribution of $O((1/N)^0)\ \Delta n_f^{(0)}$ and the solid line denotes sum of the two contributions $n_f=n_f^0+\Delta n_f^{(0)}$.

Fig.22 Temperature dependence of the conduction electrons n_c and that of the f-electrons n_f. The solid lines denote the results of the present theory and the broken lines denote the results of the slave-boson mean field theory (Refs.[14,15]).

Fig.23 Temperature dependence of the normalized magnetic susceptibility. The short dashed line denotes the bare contribution $\bar{\chi}_m^0$, the long dashed line denotes the contribution of $O((1/N)^0)\ \Delta\bar{\chi}_m^{(0)}$ and the solid line denotes the sum of the two contributions $\bar{\chi}_m\equiv\bar{\chi}_m^0+\Delta\bar{\chi}_m^{(0)}$. At T=0, $\bar{\chi}_m=\Delta\bar{\chi}_m^{(0)}=(m^*/m)_{T=0}\simeq 425$ and $\chi_m^0=0$.

Fig.24 Temperature dependence of the inverse of the normalized magnetic susceptibility $\bar{\chi}_m^{-1}$.

Fig.25 Temperature dependence of the inverse life time $1/2\tau$ of the conduction electron.

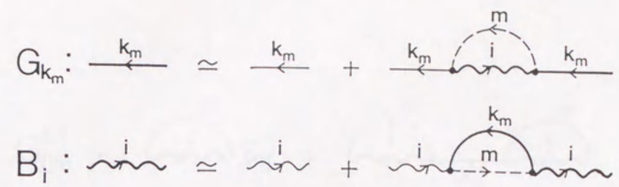

Fig. 1

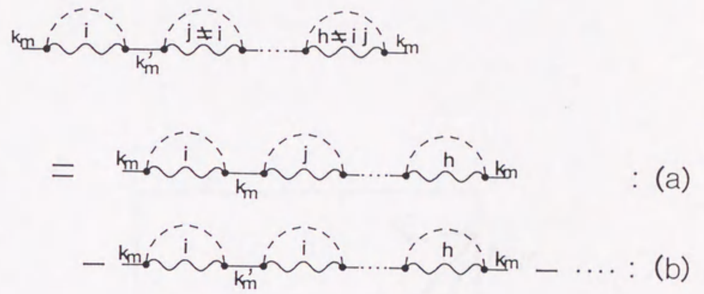

Fig. 2

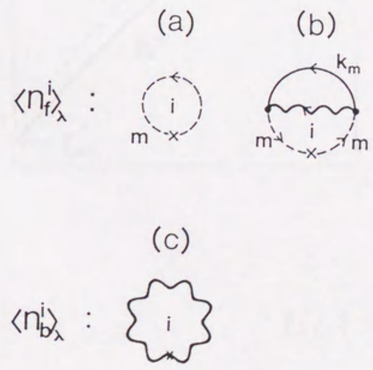

Fig. 3

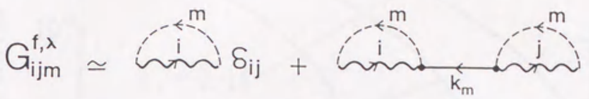
$G^{f,\lambda}_{ijm} \simeq$
m
i
δ_{ij} +
m
i
m
j
k_m

Fig. 4

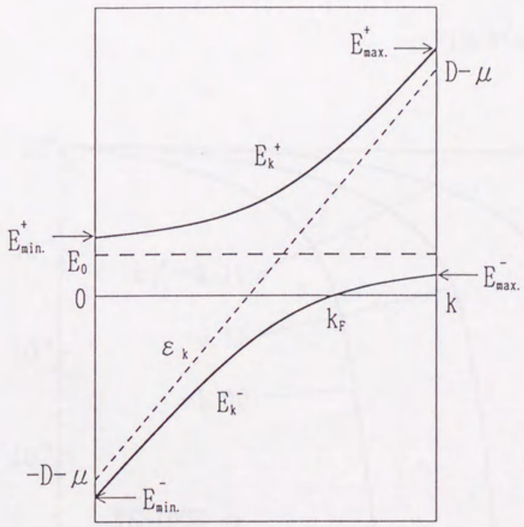
$E^+_{max.}$
D-μ
E^+_k
$E^+_{min.}$
E_0
0
$E^-_{max.}$
k
k_F
ε_k
E^-_k
-D-μ
$E^-_{min.}$

Fig. 5

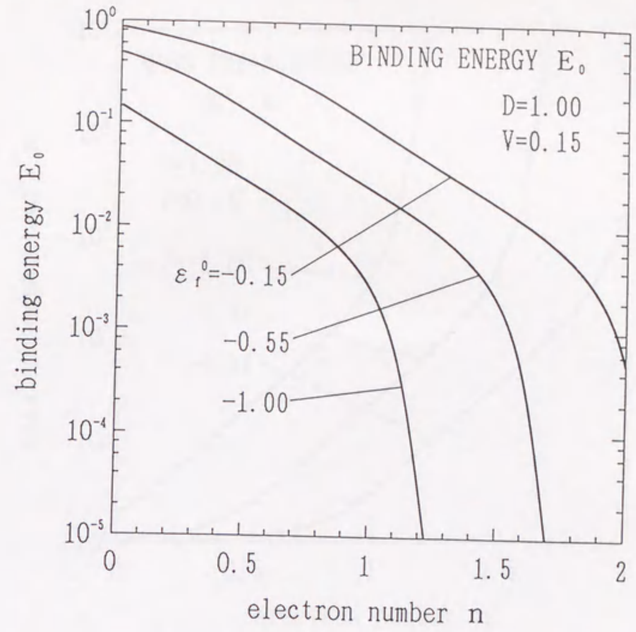
BINDING ENERGY E_0
D=1.00
V=0.15
ε_f^0=-0.15
-0.55
-1.00
binding energy E_0
electron number n
10^0
10^{-1}
10^{-2}
10^{-3}
10^{-4}
10^{-5}
0
0.5
1
1.5
2

Fig. 6(a)

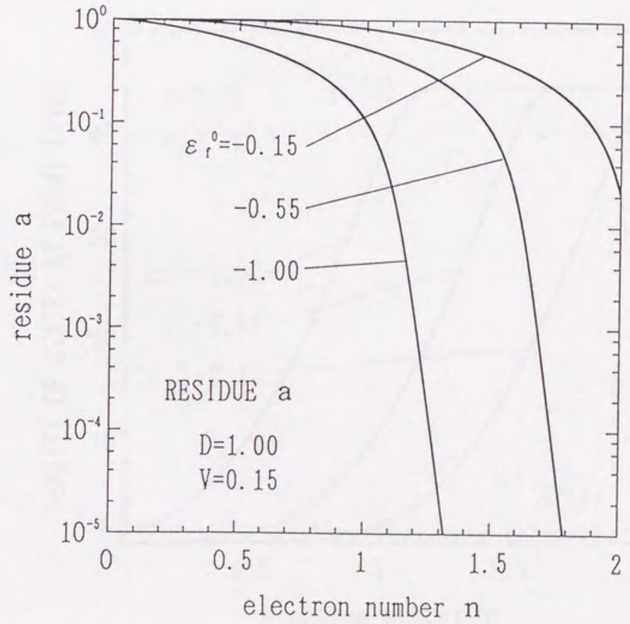
ε_f^0=-0.15
-0.55
-1.00
RESIDUE a
D=1.00
V=0.15
residue a
electron number n
10^0
10^{-1}
10^{-2}
10^{-3}
10^{-4}
10^{-5}
0
0.5
1
1.5
2

Fig. 6(b)

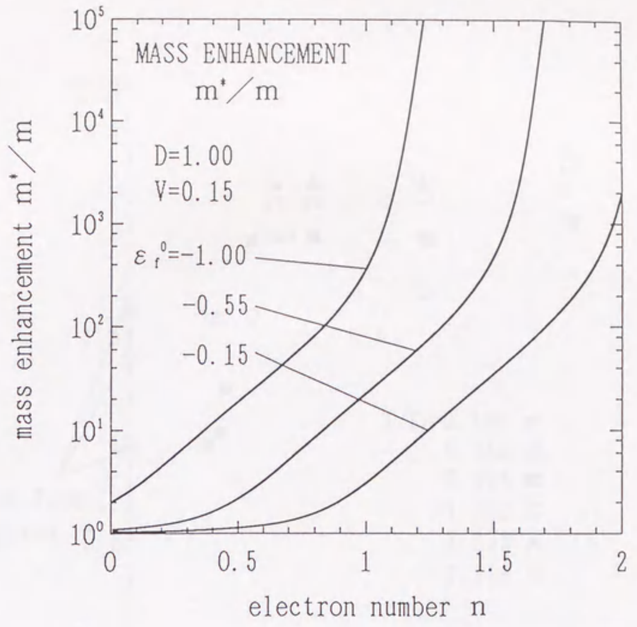
MASS ENHANCEMENT
m*/m
D=1.00
V=0.15
ε_f^0=-1.00
-0.55
-0.15
mass enhancement m*/m
electron number n
10^0
10^1
10^2
10^3
10^4
10^5
0
0.5
1
1.5
2

Fig. 7

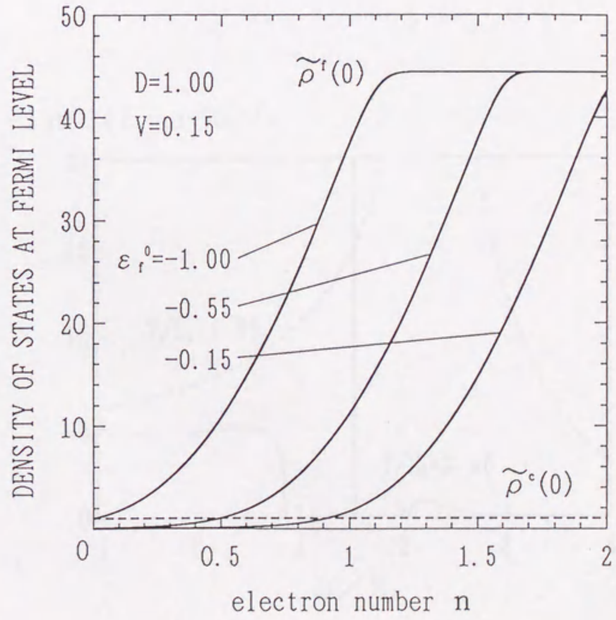
D=1.00
V=0.15
$\widetilde{\rho}^f(0)$
ε_f^0=-1.00
-0.55
-0.15
$\widetilde{\rho}^c(0)$
DENSITY OF STATES AT FERMI LEVEL
electron number n
0
10
20
30
40
50
0.5
1
1.5
2

Fig. 8

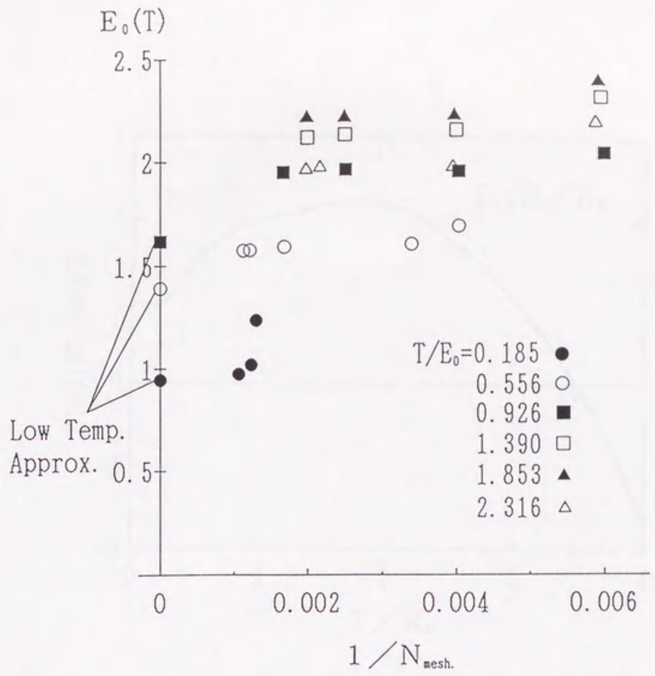
$E_0(T)$
2.5
2
1.5
1
0.5
Low Temp.
Approx.
T/E_0=0.185
0.556
0.926
1.390
1.853
2.316
0
0.002
0.004
0.006
$1/N_{mesh.}$

Fig. 9

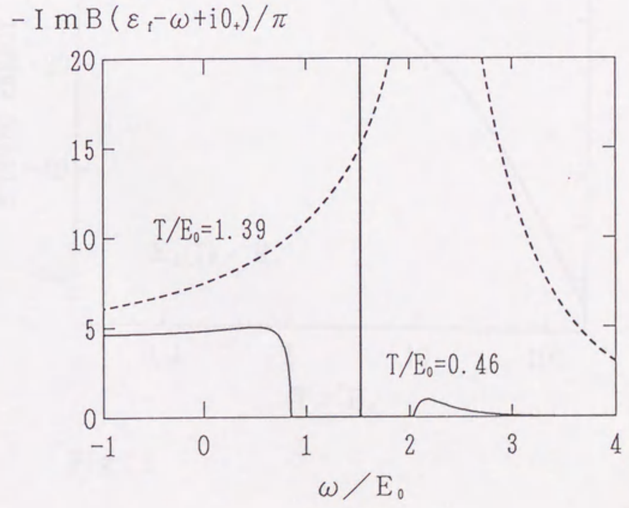
$-ImB(\varepsilon_f-\omega+i0_+)/\pi$
20
15
10
5
0
T/E_0=1.39
T/E_0=0.46
-1
0
1
2
3
4
ω/E_0

Fig. 10

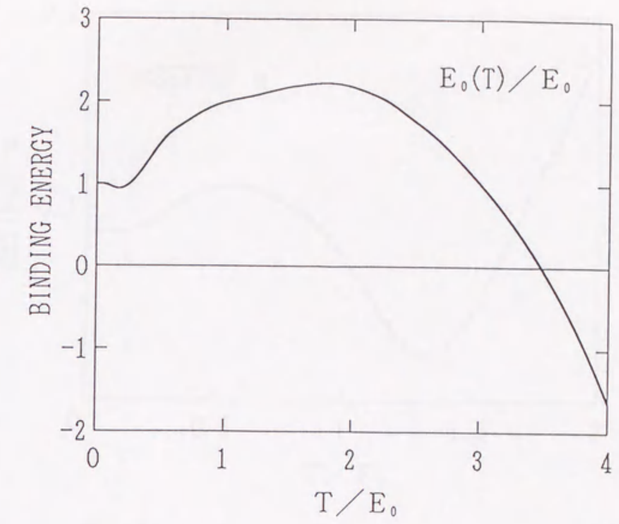
BINDING ENERGY
3
2
1
0
-1
-2
0
1
2
3
4
$E_0(T)/E_0$
T/E_0

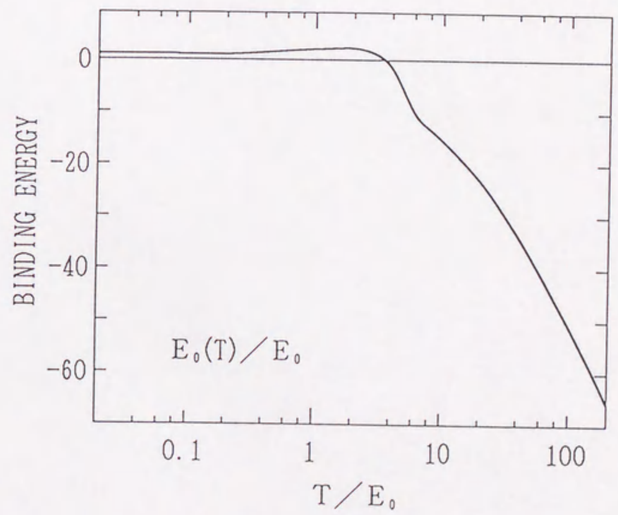
BINDING ENERGY
0
-20
-40
-60
0.1
1
10
100
$E_0(T)/E_0$
T/E_0

Fig. 11

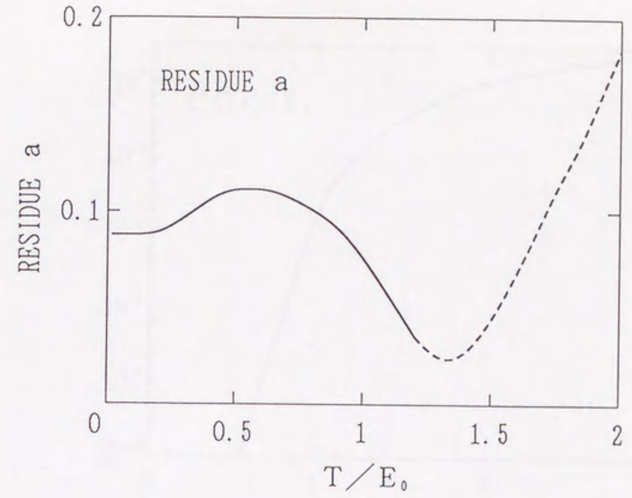

Fig. 12

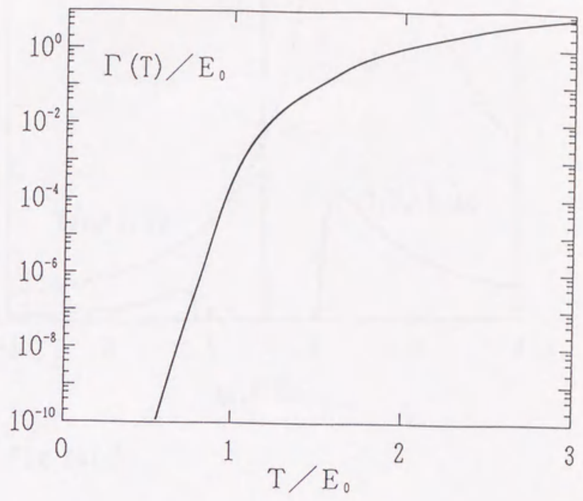
10^{0}
10^{-2}
10^{-4}
10^{-6}
10^{-8}
10^{-10}
$\Gamma(T)/E_0$
0
1
2
3
T/E_0

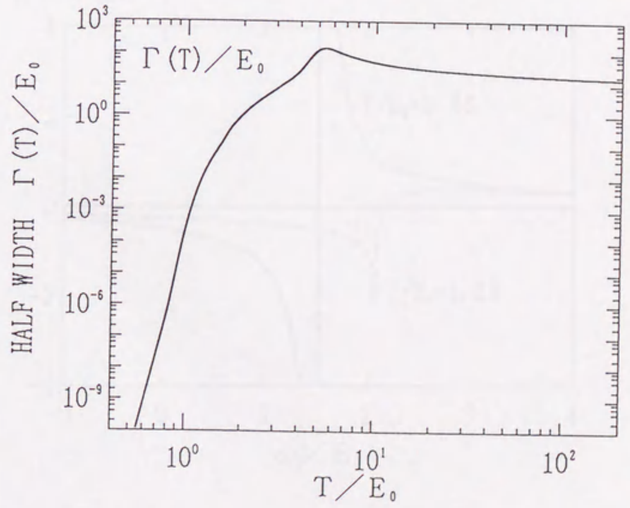
10^{3}
10^{0}
10^{-3}
10^{-6}
10^{-9}
HALF WIDTH $\Gamma(T)/E_0$
$\Gamma(T)/E_0$
10^{0}
10^{1}
10^{2}
T/E_0

Fig. 13

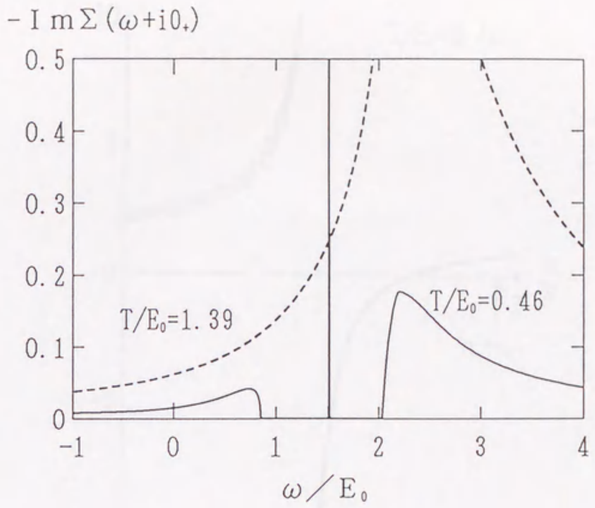

Fig. 14(a)

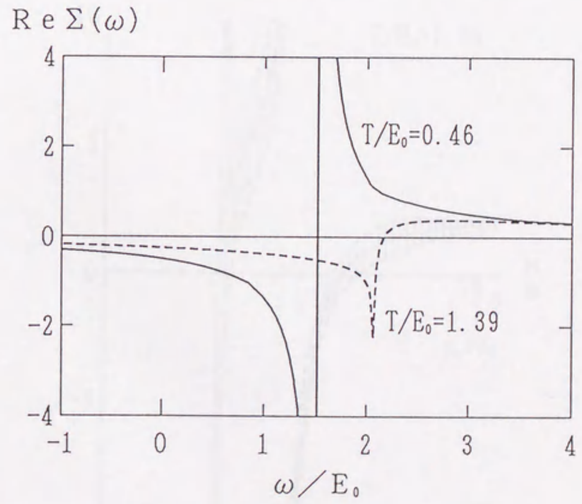

Fig. 14(b)

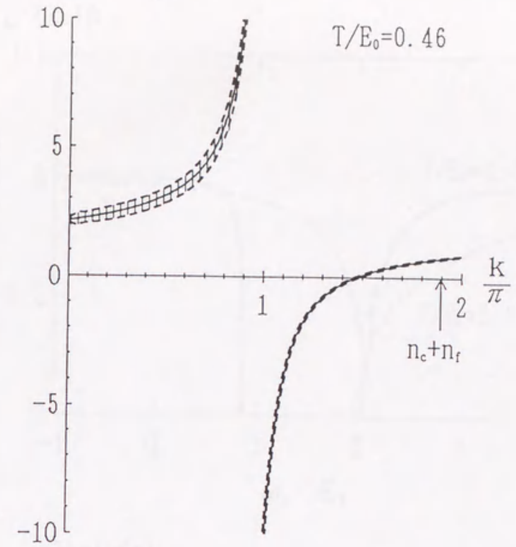
E_k/E_0 , $(E_k \pm \Gamma_k)/E_0$
10
5
0
-5
-10
T/E_0=0.46
1
2
$\frac{k}{\pi}$
n_c+n_f

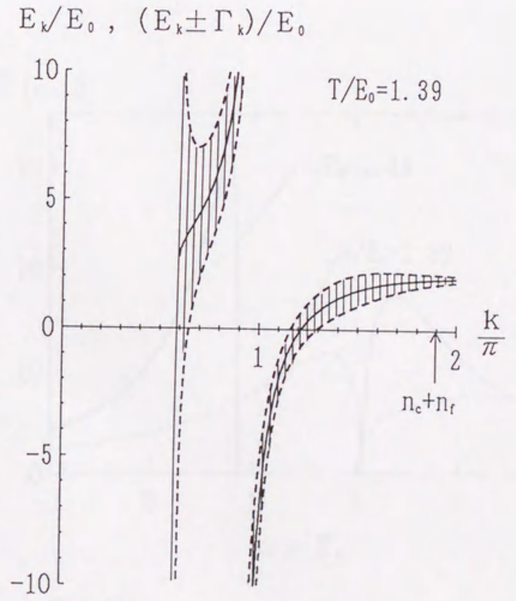
E_k/E_0 , $(E_k \pm \Gamma_k)/E_0$
10
5
0
-5
-10
T/E_0=1.39
1
2
$\frac{k}{\pi}$
n_c+n_f

Fig. 15

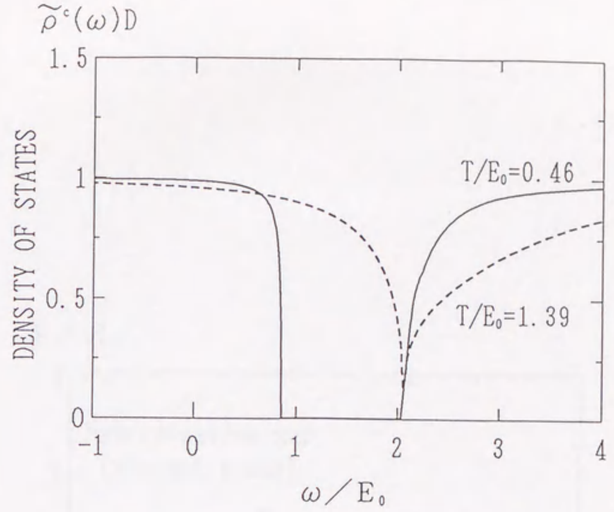

Fig16(a)

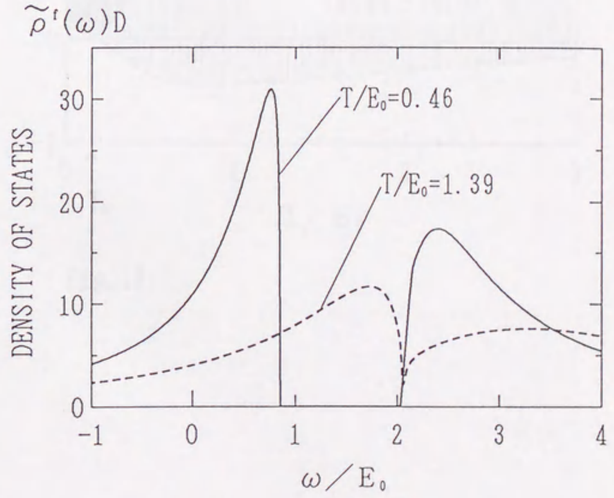

Fig16(b)

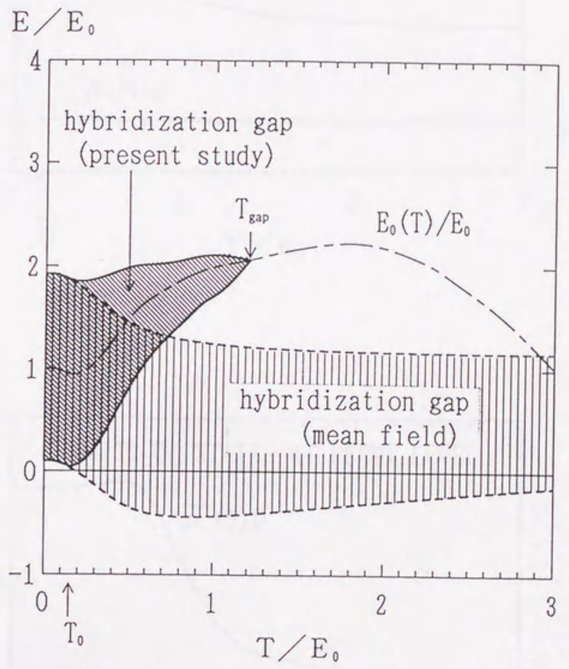
E／E₀
4
3
2
1
0
−1
hybridization gap
(present study)
T_gap
E₀(T)/E₀
hybridization gap
(mean field)
0
T₀
1
2
3
T／E₀

Fig. 17

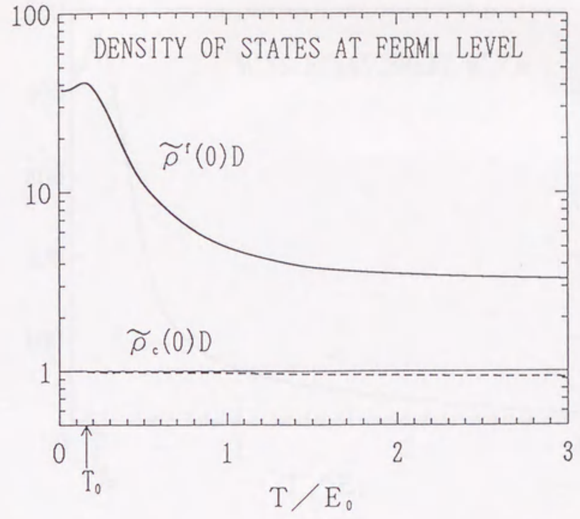
100
DENSITY OF STATES AT FERMI LEVEL
$\widetilde{\rho}^{f}(0)D$
10
$\widetilde{\rho}_{c}(0)D$
1
0
T_0
1
2
3
T/E_0

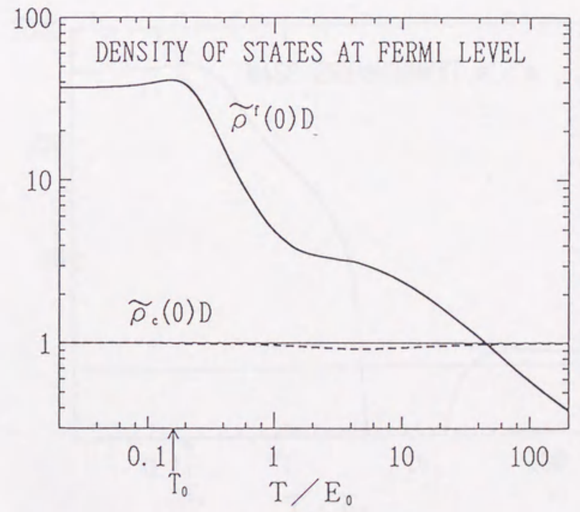
100
DENSITY OF STATES AT FERMI LEVEL
$\widetilde{\rho}^{f}(0)D$
10
$\widetilde{\rho}_{c}(0)D$
1
0.1
T_0
1
10
100
T/E_0

Fig. 18

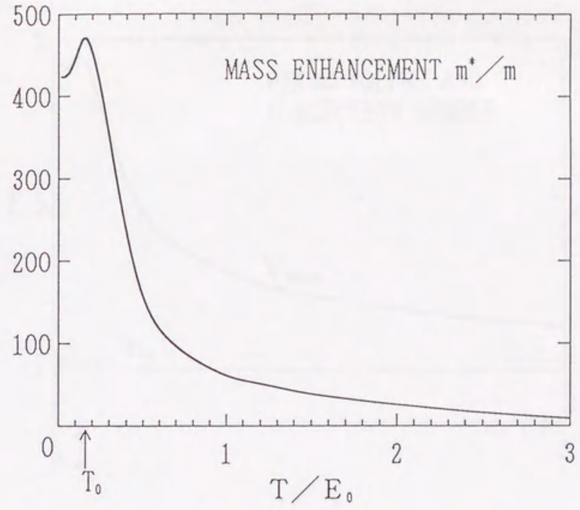
500
400
300
200
100
0
MASS ENHANCEMENT m*／m
T₀
1
2
3
T／E₀

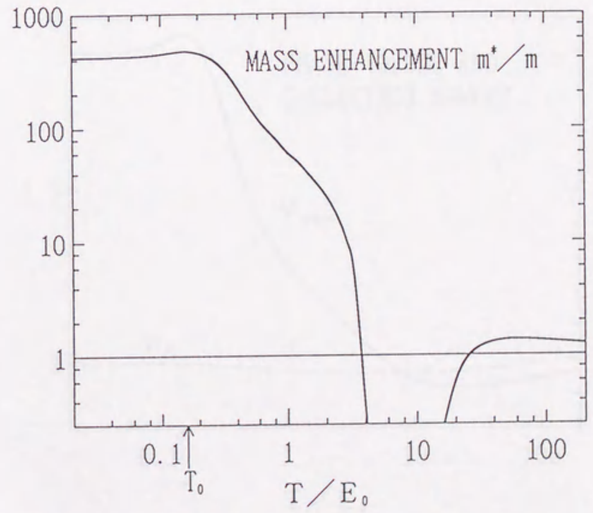
1000
100
10
1
MASS ENHANCEMENT m*／m
0.1
T₀
1
10
100
T／E₀

Fig. 19

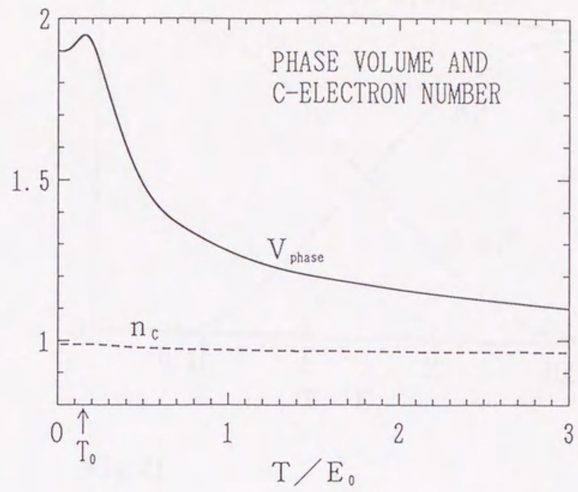
PHASE VOLUME AND
C-ELECTRON NUMBER
2
1.5
1
0
T_0
1
2
3
V_{phase}
n_c
T/E_0

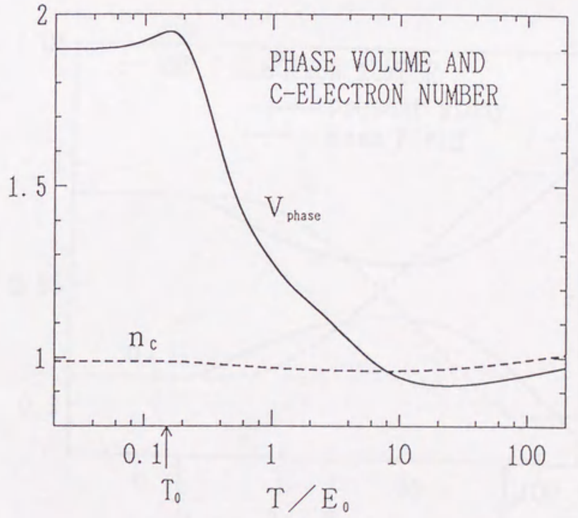
PHASE VOLUME AND
C-ELECTRON NUMBER
2
1.5
1
0.1
T_0
1
10
100
V_{phase}
n_c
T/E_0

Fig. 20

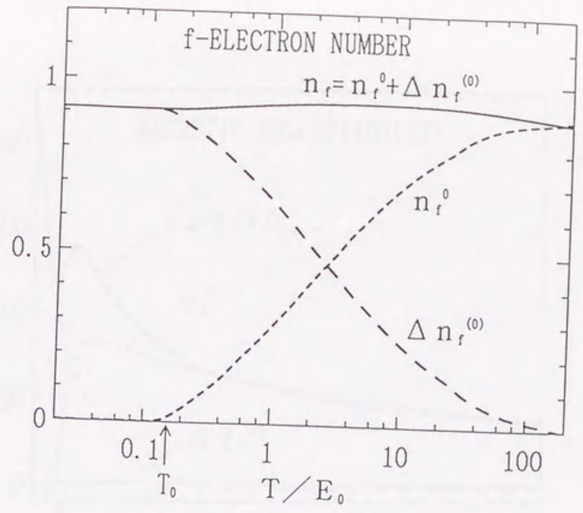
f-ELECTRON NUMBER
$n_f = n_f^0 + \Delta n_f^{(0)}$
1
0.5
0
n_f^0
$\Delta n_f^{(0)}$
0.1
1
10
100
T_0
T / E_0

Fig. 21

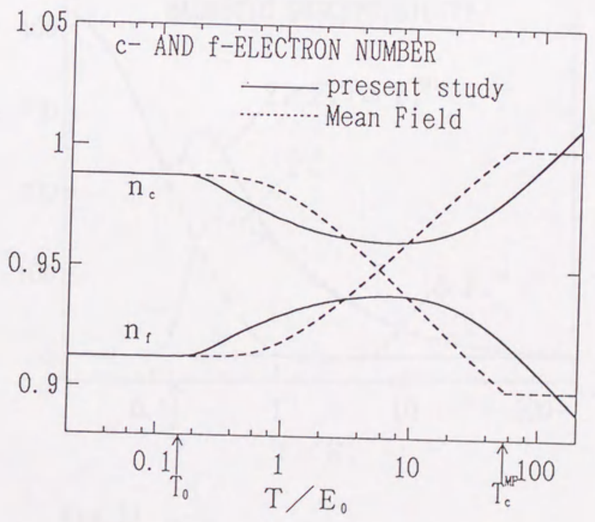
c- AND f-ELECTRON NUMBER
present study
Mean Field
1.05
1
0.95
0.9
n_c
n_f
0.1
1
10
100
T_0
T_c^{MF}
T / E_0

Fig. 22

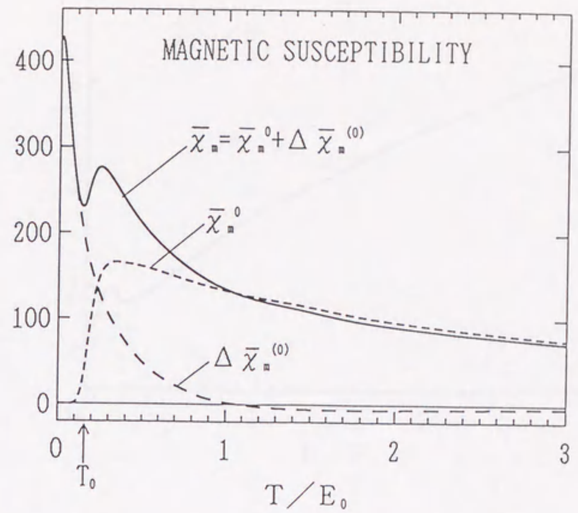
MAGNETIC SUSCEPTIBILITY
400
300
200
100
0
$\bar{\chi}_n = \bar{\chi}_n^0 + \Delta\bar{\chi}_n^{(0)}$
$\bar{\chi}_n^0$
$\Delta\bar{\chi}_n^{(0)}$
0
1
2
3
T_0
T/E_0

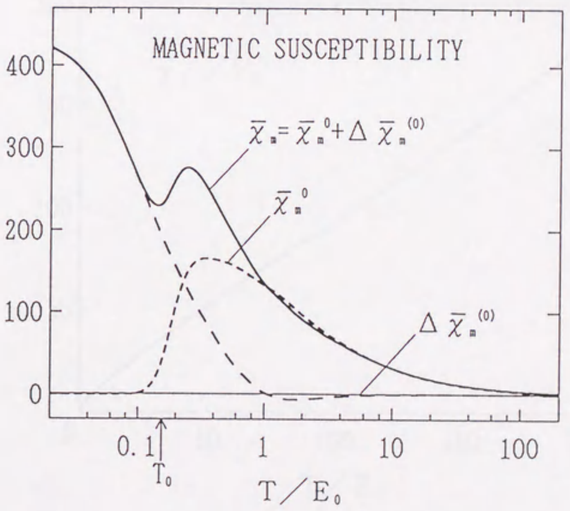
MAGNETIC SUSCEPTIBILITY
400
300
200
100
0
$\bar{\chi}_n = \bar{\chi}_n^0 + \Delta\bar{\chi}_n^{(0)}$
$\bar{\chi}_n^0$
$\Delta\bar{\chi}_n^{(0)}$
0.1
1
10
100
T_0
T/E_0

Fig. 23

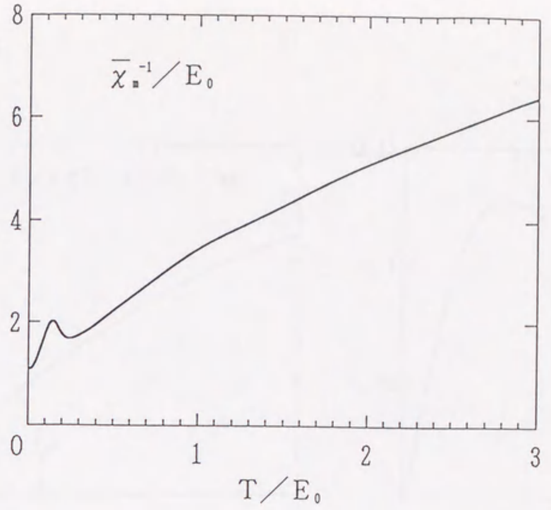
8
6
4
2
0
1
2
3
$\overline{\chi}_{\blacksquare}^{-1}/E_0$
T/E_0

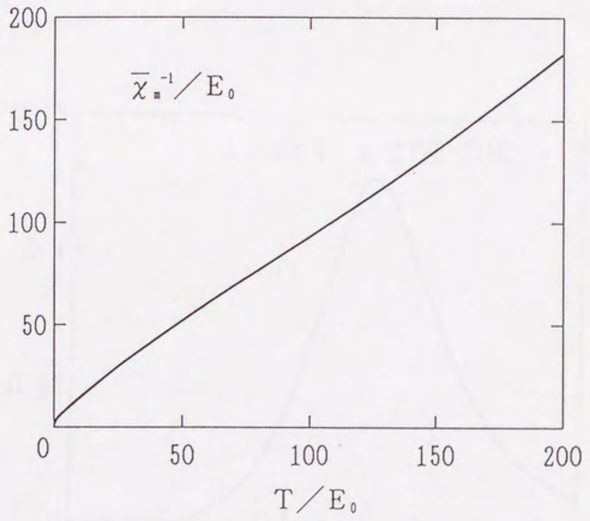
200
150
100
50
0
50
100
150
200
$\overline{\chi}_{\blacksquare}^{-1}/E_0$
T/E_0

Fig. 24

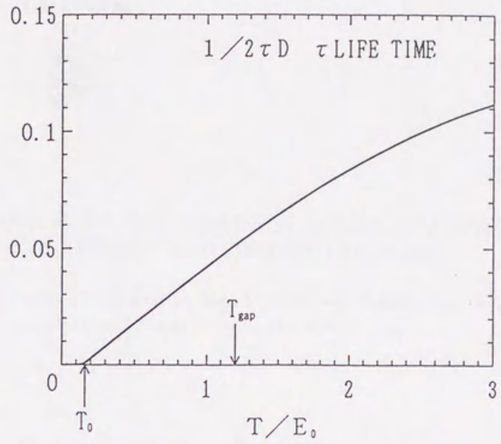
0.15
0.1
0.05
0
1 ／2τD τLIFE TIME
T_{gap}
T_0
1
2
3
T／E_0

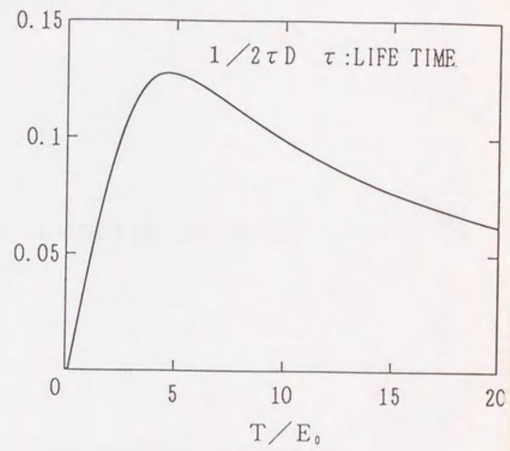
0.15
0.1
0.05
0
1 ／2τD τ:LIFE TIME
5
10
15
20
T／E_0

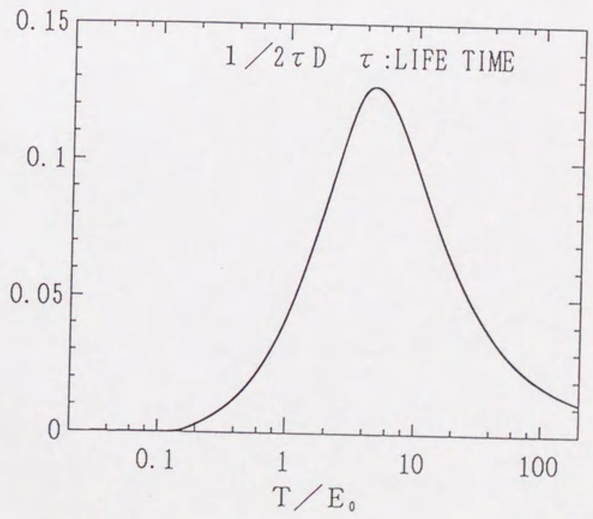
0.15
0.1
0.05
0
1 ／2τD τ:LIFE TIME
0.1
1
10
100
T／E_0

Fig. 25